

Washington University in St. Louis

Washington University Open Scholarship

Mechanical Engineering and Materials Science
Independent Study

Mechanical Engineering & Materials Science

1-11-2019

Design of the WUFR-19 FSAE Suspension

Alex Levy

Washington University in St. Louis

James J. Potter

Washington University in St. Louis

Follow this and additional works at: <https://openscholarship.wustl.edu/mems500>

Recommended Citation

Levy, Alex and Potter, James J., "Design of the WUFR-19 FSAE Suspension" (2019). *Mechanical Engineering and Materials Science Independent Study*. 83.

<https://openscholarship.wustl.edu/mems500/83>

This Final Report is brought to you for free and open access by the Mechanical Engineering & Materials Science at Washington University Open Scholarship. It has been accepted for inclusion in Mechanical Engineering and Materials Science Independent Study by an authorized administrator of Washington University Open Scholarship. For more information, please contact digital@wumail.wustl.edu.



Washington University in St. Louis

SCHOOL OF ENGINEERING & APPLIED SCIENCE

Fall 2018 MEMS 400 Independent Study Project

Design of the WUFR-19 FSAE Suspension

Alex Levy – B.S. Mechanical Engineering '20

Advisor: Dr. James Jackson Potter – Faculty Dept. of Mechanical Engineering

Contents

Abstract.....	4
1 Wash U Racing	4
1.1 Role of a Suspension	4
1.2 WUFR-19 Suspension	5
2 The FSAE Challenge and Constraints.....	5
2.1 The Events	6
2.2 Team Constraints	9
2.3 System Constraints	9
3 Resources and Software for Design	10
3.1 Research Library.....	10
3.2 Software Catalog.....	11
4 Car and Sensor Data.....	12
4.1 Collected Sensor Data	12
4.2 Basic Car Weight Parameters – BFR18.....	13
5 Tires and Tire Data	13
5.1 Tire Selection.....	13
5.2 Tire Data.....	14
5.3 Application of Tire Data	19
6 Suspension Geometry	23
6.1 Front View Geometry.....	23
6.2 Additional Points and Steering Geometry	33
7 OptimumKinematics Results	34
Going Forward	42
Appendix A: Additional Technical Information.....	42
A.1: Spring Rates	42
References	43

List of Figures

Figure 1: A Top View of a Double Wishbone Suspension with Toe Link [2, p. 643] 5

Figure 2: WashU Racing's BFR18 Double A-Arm Suspension 5

Figure 3: The Skid Pad Schematic as Provided in the 2019 Rules [3, p. 123]..... 8

Figure 4: The Autocross Schematic as Provided in the 2019 Rules [5] 8

Figure 5: The 2018 Endurance Track from FSAE Michigan [6] 9

Figure 6: The Cardinal Planes for SU-93001-BA in SolidWorks 11

Figure 7: As an example, the 2019 Front Suspension Modeled in Optimum Kinematics 12

Figure 8: The Definition of a Tire Slip Angle [1, p. 14]..... 15

Figure 9: The De-Identified Graph of Lateral Force Against Slip Angle for the R25B 18.0x7.5-10 [23] 16

Figure 10: The De-Identified Graph of Instantaneous Cornering Stiffness Against Lateral Force for the R25B 18.0x7.5-10 [23] 17

Figure 11: The De-Identified Graph of Instantaneous Cornering Stiffness Against Slip Angle for the R25B 18.0x7.5-10 [23]..... 17

Figure 12: Aligning Torque on the Footprint of a Tire [2, p. 70] 18

Figure 13: The De-Identified Graph of Aligning Torque Against Slip Angle for the R25B 18.0x7.5-10 [23] 19

Figure 14: The Bicycle Model [2, p. 127]..... 20

Figure 15: The Steer Camber Curve for the 1.2g Left Turn..... 21

Figure 16: The Front and Rear Wheel Center Planes Set a Distance Apart by the Wheelbase 23

Figure 17: The Pitch Motion Loaded in to OptimumKinematics 24

Figure 18: SU-93001-BA with Front and Rear Track Planes on Both Sides of the Car 28

Figure 19: A Roll Center Height on a Suspension Geometry [2, p. 614]..... 29

Figure 20: The Front View Swing Arm [2, p. 628]..... 30

Figure 21: The Heave Camber Change Rate..... 31

Figure 22: The Roll Camber Change Rate 31

Figure 23: The Final Front-Front View Geometry..... 32

Figure 24: The Final Rear-Front View Geometry..... 32

Figure 25: Important Placement of Components within the Wheel..... 33

Figure 26: The Steer Camber Curve 34

Figure 27: The Heave Motion Modeled in OptimumKinematics..... 34

Figure 28: The Roll Motion Modeled in OptimumKinematics 35

Figure 29: A Front View of WUFR-19's Front Suspension Modeled in OptimumKinematics 35

Figure 30: A Top View of WUFR-19's Front Suspension Modeled in OptimumKinematics..... 36

Figure 31: A Front View of WUFR19's Rear Suspension Modeled in OptimumKinematics..... 36

Figure 32: A Top View of WUFR-19's Rear Suspension Modeled in OptimumKinematicsc 36

Figure 33: A Graph of Front Left Camber Gain [deg] Against the Heave Motion [in] 37

Figure 35: A Graph of Front Left Camber Gain [deg] Against the Pitch Motion [deg] 37

Figure 36: A Graph of Front Left Camber Gain [deg] Against the Roll Motion [deg] 38

Figure 37: A Graph of Rear Left Toe Angle [deg] Against the Heave Motion [in]..... 38

Figure 38: A Graph of Rear Left Toe Angle [deg] Against the Pitch Motion [deg]..... 39

Figure 39: A Graph of Rear Left Toe Angle [deg] Against the Roll Motion [deg]..... 39

Figure 40: A Graph of Front Left Motion Ratio [unitless] Against the Heave Motion [in] 40

Figure 41: A Plot of Wheel Rate [lbs/in] with Varied Motion Ratio [unitless] and Constant Spring Rate..... 40

Figure 42: A Graph of the Front Left Motion Ratio [unitless] Against the Pitch Motion [deg].....	41
Figure 43: A Graph of the Front Left Motion Ratio [unitless] Against the Roll Motion [deg].....	41
Figure 44: A Graph of the Front Kinematic Roll Center Position in Z [in] Against Y [in] Under the Roll Condition	42
Figure 45: A Graph of the Rear Kinematic Roll Center Position in Z [in] Against Y [in] Under the Roll Condition	42

List of Tables

Table 1: The Maximum Values Captured on the Sensor CAN Bus During Fall 2018 Testing	12
Table 2: The Available Hoosier Tires for the 2019 Design Year [21]	14
Table 3: The Yaw Velocity for WUFR-19.....	21
Table 4: The Parameters for Lateral Force and Cornering Stiffness Calculations	21
Table 5: Camber Values for Max Steering Lock for a Left Turn with 1.2g's of Lateral Acceleration	22
Table 6: The Maximum Lateral Force Capability of Each Tire Under Steer	22
Table 7: The Cornering Stiffness Values for Each Tire in Steer.....	22
Table 8: The Slip Angles for the 1.2g Left Turn	22
Table 9: The Lateral Acceleration and Load Transfer Using the Target Time Method.....	26
Table 10: The Lateral Load Transfer on the Inspection Tilt Test.....	26
Table 11: The Lateral Load Transfer for the Third Method of Taking a High Speed Hairpin Turn .	26
Table 12: The Maximum Center of Gravity Height for Different Load Conditions	27
Table 13: The Minimum Required Trackwidth for the Desired Load Transfer with the Calculated Center of Gravity Height.....	28
Table 14: The Roll Center Heights with Rolling and Nonrolling Moments.....	30
Table 15: FVSA and Camber Characteristics for the Front and Rear	32
Table 16: The Steer Camber Characteristics for the Front Suspension	33

Abstract

This report outlines the rationale and design constraints for Wash U Racing's WUFR-19 suspension for the 2019 FSAE Michigan competition. This includes competition rules, team design goals of drivability and control, and compliance with good engineering practices. To stay competitive, the team has reinvented the design philosophy of the car for the 2019 season, highlighting the use of multiple software packages and several parallel problem-solving methods when possible. The system was designed using MATLAB, SolidWorks, and OptimumKinematics racing software. Simulations were created to evaluate the car's grip potential through heave, pitch, roll, and steer motions. These results were compared with tire data models to tune for improved control at peak conditions. Additionally, kinematic equations were used along with sensor data from past iterations of Wash U Racing projects to alternatively predict handling capabilities for the new platform. This paved the way for the creation of front and rear geometries in SolidWorks to be the basis for the WUFR-19 chassis and the rest of the project development.

1 Wash U Racing

Operating out of the Internal Combustion Laboratory on the ground floor of Jolley Hall on the Danforth Campus, Wash U Racing has expanded considerably since its revival in 2011. As of the 2019 development season, the team boasts a membership of nearly 80 members from all engineering disciplines within the School of Engineering and Applied Sciences, as well as students from the Sam Fox School, the Olin School of Business, and the College of Arts and Sciences. As a result of this size, the team has adopted a leadership structure with 5 members of an elected executive board collaborating with appointed system leads. These executive members are the President, Chief Engineer, Treasurer, Vice President, and Recruitment Chair. Additionally, the team is split into 8 systems: Electronics, Data Acquisition, Aerodynamics and Composites, Powertrain, Drivetrain, Ergonomics, Manufacturing, Chassis, and Suspension. Each system has one or two leads that oversee the design and build of each division of the project. For the 2019 design year, Wash U Racing is changing its platform and evolving the architecture within our FSAE product. Last year's car, the Bears Formula Racing 18 (BFR18) car will become the Wash U Formula Racing 2019 (WUFR-19).

1.1 Role of a Suspension

In racing, a suspension has two critical functions: to guide the motion of the chassis and to control the contact patch of the tire on the ground. Additionally, there are three main goals in the design of a good racing suspension system: independence across each corner, control of tire behavior in transient conditions, and reducing compliance throughout the system [1, p. 43]. To achieve the first goal, a 5-bar linkage setup should be used with two wishbones and a toe link controlling four out of 5 degrees of freedom of a wheel. With this setup in place, the wheel can only spin in the direction of motion but is resisted in all other planes. For the front suspension, the toe link is replaced with a tie rod attached to a steering rack to turn the wheels. Additionally, a 6th member is added to actuate the push-pull spring and damper system. This works towards the first main function of controlling and mitigating eccentric chassis motion as the car moves.

Unlike in commercial automotive design, peak comfort and effortless driver input are not top priorities, especially at the cost of speed and control. As a result, the design of racing geometry is highly unique to each competition, team, and car. To achieve the first goal of chassis control, race cars are designed to be very stiff in both component structure and tune. When the chassis and structural components are designed to be "infinitely stiff" the suspension can be tuned. If the frame has significant compliance during ride, changes to the suspension will be felt by the driver.

Additionally, the suspension design must incorporate a thorough understanding of tire performance and capability to ensure that camber and normal load conditions are aligned correctly.

1.2 WUFR-19 Suspension

Wash U Racing uses a short long arm (SLA) double wishbone suspension (also called A-arm or control arms). This is a lightweight independent setup that allows for easy adjustment and near total customizability. It is the most common setup in the professional and amateur racing worlds. A theoretical example is shown in Figure 1.

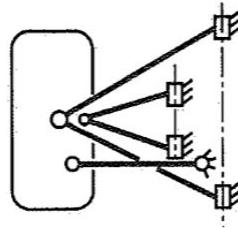


Figure 1: A Top View of a Double Wishbone Suspension with Toe Link [2, p. 643]

Additionally, Figure 2 shows the BFR18's double wishbone suspension from the previous model year.



Figure 2: WashU Racing's BFR18 Double A-Arm Suspension

2 The FSAE Challenge and Constraints

Since 2011, Washington University in St. Louis has attended FSAE Michigan, one of the largest student design competitions in the world, where students design, build, and race formula-style racecars in a single school year. Over 120 teams from around the world travel to Michigan International Speedway to collaborate with, learn from, and compete against other students while receiving feedback from distinguished design judges from the automotive industry. Ultimately, one of the largest challenges for Wash U Racing competing at FSAE is balancing good engineering with creating the fastest car possible. In other words, it is crucial to the design process that

everything is tested and validated before it can go on the project, even if that slows advancement in dynamic events in the long run.

2.1 The Events

Over the course of four days in May, the WUFR-19 must pass through rigorous technical inspections, 3 static events, and 4 dynamic events - each meant to evaluate a different aspect of the project. They will be described in detail in the following sections.

2.1.1 Inspections

Before advancing to any of the events at competition, our car must pass a sound test, brake test, tilt test, and general technical evaluation. The sound and brake test are overseen by the powertrain and ergonomics teams respectively and will not be covered in this report.

To pass the tilt test, the car must not leak fluids when raised to an angle of 45 degrees from horizontal, and all four wheels must stay in contact with the test rig when raised to 60 degrees. This test ultimately simulates the car experiencing 1.7g's of lateral acceleration [3, p. 104]. Preparation for this test will be discussed in later sections of the report.

In the general technical inspection, the team must be able to prove our compliance with any and all regulations listed in the official Formula SAE Rules 2019 document. In general, each system on the team is responsible for ensuring that the design and assembly of their own system is in accordance with all regulations. The President and Chief Engineer must oversee this process and ensure that general rules are satisfied, and all systems are thorough. For easy reference and concision, the relevant rules to suspension and steering will be recreated here:

“T.1.2 Wheelbase [3, p. 18]

T.1.2.1 The vehicle must have a wheelbase of at least 1525 mm.

T.1.3 Vehicle Track [3, p. 18]

T.1.3.1 The track and center of gravity must combine to provide adequate rollover stability.

T.1.3.2 The smaller track of the vehicle (front or rear) must be no less than 75% of the larger track.

T.1.5 Suspension [3, p. 19]

T.1.5.1 The vehicle must be equipped with a fully operational suspension system with shock absorbers, front and rear, with usable wheel travel of at least 50 mm, with a driver seated.

T.1.5.4 Fasteners in the Suspension system are Critical Fasteners, see T.10.2 and T.10.3

T.1.7 Wheels [3, p. 20]

T.1.7.1 Wheels must be 203.2 mm (8.0 inches) or more in diameter.”

All of these things are considered in the design of the platform for the year. Note again that these are abridged rules relevant to the suspension and steering systems and any future designers should consult the full regulations for the model year, available through FSAE online.

2.1.2 Static Events

The competition has three static events: Business, Cost, and Design. The Business and Cost presentations are outside the scope of this report. The Design competition, however, is a critical component of FSAE Michigan and accounts for 150 of the 1000 available points [3, p. 109]. At this event, each system lead pairs with a professional engineer from their relevant discipline and

explains all critical components of the system, design rationale, validation, and answers questions. For Wash U Racing this has been one of the toughest portions of the competition. The design judges expect to see professional, thorough design based off of quantitative data collection, validated simulation models, and careful testing protocols. Specifically, the Formula SAE Design Judging Score Sheet [4, p. 2] says:

“REMEMBER: Judges are not just scoring your vehicle. They are scoring your knowledge and understanding of vehicle development and performance. Reflective of this, for each physical design category (**Suspension, Frame/Body/Aero, Powertrain, and Cockpit/Controls/Brakes/Safety**) judges evaluate the team’s development process. Generally, each category is judged with the following emphasis:

- Design (25%): Assessment of design process used by team. Is this a new design, evolution, or complete carryover? Were different design options considered? Were appropriate pre-build analyses performed?
- Build (25%): Does the physical specimen presented reflect the early design work? Is it reflected in design report? If not, why not? What special manufacturing considerations were encountered?
- Refinement/Validation (25%): How thorough and honest has the team been about testing? Was a test plan developed and executed? Were discrepancies between predicted and tested results documented and acted upon to improve final build?
- Understanding (25%): Is the team that presents the car at competition truly intimate with the design? Can they quickly give detailed answers about any subsystem? Or do they have to “go ask someone else”?”

This section emphasizes the judge’s commitment to ensuring the system leads and designers are aware of why and how we are designing our components, not just that we are creating parts/systems. Specifically, the judges and competitors are provided with some baseline questions that we should be able to answer. They also serve as the jumping off point for our explanations and the judges’ additional examination. Those questions, in their entirety, are reprinted here [4, p. 3]:

- “Does the team understand vehicle dynamics fundamentals?
- What methods were used for selecting tires and sizes?
- How was the handling, response and tractive capability of the tires considered in the design of the suspension?
- What analysis methods were used in the development of wheel base, weight distribution, c.g. height, front and rear track widths, roll axis location (static and dynamic), camber gain curves, link lengths, Ackermann, anti-squat/dive, king pin inclination scrub radius, bump steer, and other geometry/kinematics?
- Have peak loads been determined and designed for?
- Have appropriate materials and heat treatments/coatings been selected for their function?
- Have attachments been properly analyzed and implemented? (e.g., no rods-ends in bending, double shear joints, etc)
- How were dampers selected and how are they valved?
- How were wheel rates and roll resistance values developed/determined?
- Has every effort been used to reduce unsprung mass?
- Have adjustments been provided for different competition environments?
- Has system friction, hysteresis and bearing lubrication been addressed?
- Do suspension/steering links and hardware have excessive compliance?
- Have predicted handling characteristics been validated? If so, How?”

This report will outline answers to some of these questions for the WUFR-19c suspension.

2.1.3 Dynamic Events

The Dynamic portion of the competition represents an aggregate 675 points: Acceleration (100 points), Skid Pad (75 points), Autocross (125 points), Efficiency (100 points), Endurance (275 points) [3, p. 119].

The Acceleration event is a test of the car's engine output, driveline efficiency, overall torque, and longitudinal tire grip. The drivers must launch off of a starting line and drive as quickly as possible down a 75-meter straightaway [3, p. 123].

The Skid Pad event is designed to test the car's lateral grip, handling, and control around a tight figure 8 track. The dimensions of the track are pictured in Figure 3.

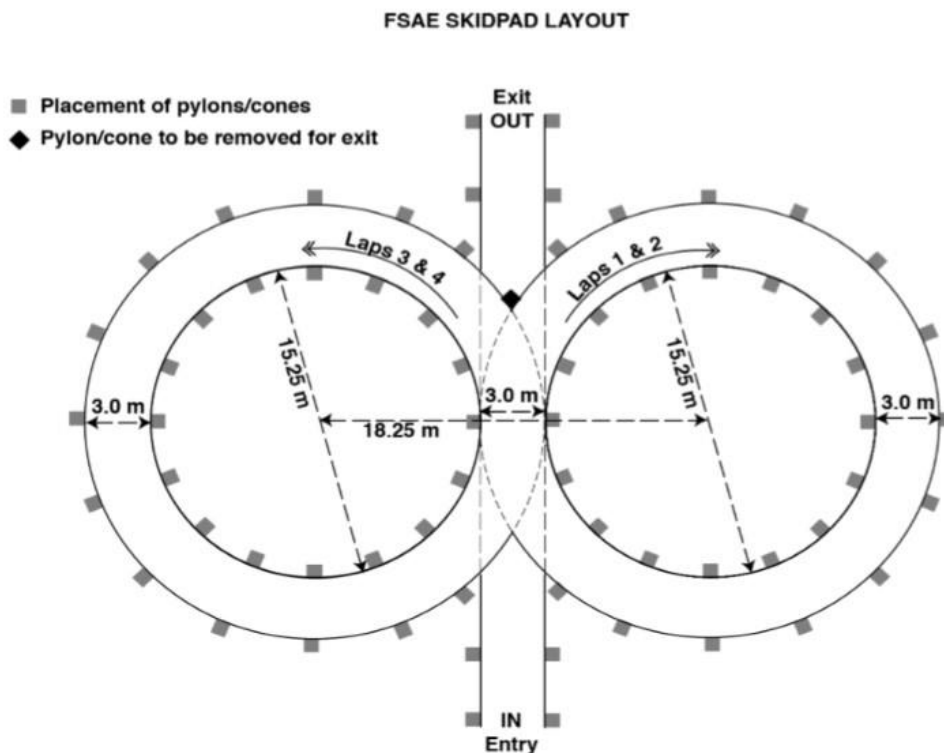


Figure 3: The Skid Pad Schematic as Provided in the 2019 Rules [3, p. 123]

Additionally, the third event is a fast-lap around an autocross track. This event is meant to test everything that the car can do: quick slaloms, short burst straights, and tight hairpin turns. Results from the autocross determine running order for the final endurance event and are crucial to overall performance at competition. The 2018 Autocross track is pictured in Figure 4.

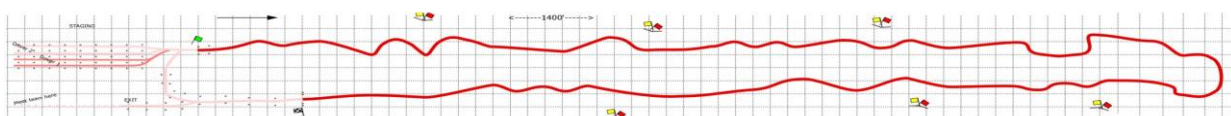


Figure 4: The Autocross Schematic as Provided in the 2019 Rules [5]

The final dynamic event is the 22-kilometer endurance race. This is the only event that sees multiple cars on the track at the same time. It is set on a similar style track to autocross and is meant to challenge multiple aspects of the car's performance, with the added difficulty of validating the fatigue strength of the car. After 11 laps, the car must pull into a run-off area, turn-off, one driver must egress, another has to be strapped in, and the car must restart. Many teams from the top and bottom of the score sheet have had cars fail during this event either due to components breaking or the car not starting after the midway break. The 2018 endurance track is pictured in Figure 5.

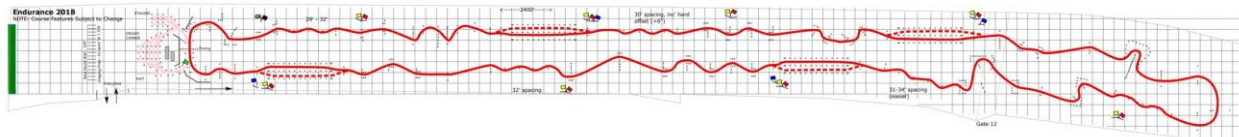


Figure 5: The 2018 Endurance Track from FSAE Michigan [6]

2.2 Team Constraints

For the 2019 season, Wash U Racing set a team-wide goal to improve drivability and control. This is the leading design constraint for all conditions and parameters of the car. As a result, in the balance between lightweight packaging and superior drivability, we selected every decision that increased control. Additionally, every parameter selected for the geometry and all mechanical components for the year should draw their ultimate reasoning back to this goal. For example, the stiffness parameters for the front and rear bell cranks should be set based on reducing the variation in motion ratio under high loading. If the part experiences high deflection, the motion ratio will diverge from the simulation results and the car's response will become unpredictable. As a result, even at the cost of marginal weight, stiffness for these components was prioritized.

2.3 System Constraints

The team constraint of drivability produced five internal suspension constraints for the design year: an increase in stability and control, the creation of custom tunes for each event at competition, the validation of more characteristics of the 2018 car, the validation of additional characteristics on the new 2019 chassis, and the development of an understanding of compliance effects on understeer and oversteer response.

First, to increase driver control the team has aimed to reduce bump steer. This is unwanted toe angle variation during vertical travel of the wheel. It is specifically an issue in the rear suspension where the chassis-grounded toe link should constrain this degree of freedom. On BFR18, the toe link was designed parallel to the upper control arm and resulted in excessive (upwards of 5 degrees positive and negative) compliance steer. Additionally, the new design will reduce toe and camber compliance under squat (acceleration induced longitudinal load transfer to the rear) and dive (brake induced longitudinal load transfer to the front). Finally, we have used tire data and an understanding of lateral force to maximize grip in turn to increase overall track velocity through corners.

Second, the new geometry and software models have allowed for the creation of new static alignments for each of the dynamic events at competition. Specifically, a better understanding of camber and toe variation curves, as well as tire data, has allowed for the creation of event-specific shims to quickly adjust grip for the demands of each event. These setups will be used in conjunction with more in-depth damper and anti-roll bar settings to completely retune the car for each driver's preference.

Third, support from the Mechanical Engineering and Material Science department at Washington University, as well as MicroMeasurements VPG and Texsense Sensors have allowed for the implementation of accelerometers, gyroscopes, and potentiometers to validate many of the parameters of the 2018 car during Fall 2018 testing. These data were used in parallel calculations between the 2018 and 2019 platforms to try to match the validity of models. All calculations were done for the 2018 and 2019 cars simultaneously and the theoretical results for the 2018 chassis were compared to the collected sensor values. This helped to refine and validate several problem-solving methods.

Fourth, the team plans to carefully remeasure and remodel every physical node on the 2019 chassis, as well as all manufactured parts to create a second “fabricated” simulation of the car. Essentially, the goal is to see what variation in manufacture and assembly is avoided and how much tolerances can impact predicted response of key parameters.

Fifth, having a more predictable geometry will allow for the creation of a stacked compliance gradient to predict oversteer and understeer effects under different loads. Every part and node on the car will deform some amount under loading, however, understanding how some components comply in parallel and series will determine the overall allowable deflection of each macro assembly, as well as the car’s prescribed response to that nonlinearity. For example, the team is working to model how much overall deflection can travel through the hub, upright, and upright adapter assembly before parts fail out of tolerance or performance in a given simulation has a noticeable divergence. This deflection limit would then be set as the overall upper bound for the assembly and stiffness would be allocated to each component as necessary for the lightest composite system.

The final design constraint within the suspension system for the 2019 design year is the 10” OZ Magnesium Center Lock wheels that were selected to cut unsprung weight. The rules require a minimum 8” diameter wheel, however, these would require extensive custom fabrication of wheel barrels, wheel centers, brake calipers, and other complex components. This goal did not fit within the team’s yearly priorities or timeline so the 10” wheels were selected. The previous 13” wheels were too large and too heavy for competitive racing applications.

3 Resources and Software for Design

3.1 Research Library

Doing research on FSAE and racing in general is different than most other topics because many supposed “experts” in the field, and much of the “advice” that can be found is not based in engineering design as much as gut intuition. This includes many daunting outlets like FSAE.com and other amateur racing forums. Additionally, many books about vehicle dynamics and the tuning/design of cars are not applicable to a race car with different demands.

Moreover, one should resist looking at other team’s designs, papers, and technical information for anything more than inspiration. Other teams have different design goals, unique constraints, and are sometimes wrong in their design or rationale.

One of the best places to begin research is Race Car Vehicle Dynamics by William and Doug Milliken, in addition to the follow texts:

- Race Car Vehicle Dynamics by William and Douglas Milliken [2]
- Tune to Win by Carroll Smith [1]
- Prepare to Win by Carroll Smith [7]

- Engineer to Win by Carroll Smith [8]
- Suspension Geometry and Computation by John Dixon [9]
- Automotive Chassis Engineering by David Band John Fieldhouse [10]
- Vehicle Dynamics by Reza Jazar [11]
- The Tyre as Sensor to Estimate Friction by Willem Pasterkamp [12]
- Automobile Tyres by L.J.K Setright [13]
- The Shock Absorber Handbook by John Dixon [14]

3.2 Software Catalog

3.2.1 MATLAB

Design of the 2019 suspension began in MATLAB R2018a. All coded calculations are contained in the document: *Determination_of_Suspension_Parameters_and_Design.m* [15]. This includes the rationale for track width, wheel base, load transfer constraints, body roll estimations, and steering camber curves among others. This will be expanded on in each relevant section. MATLAB was an efficient choice as it allowed for complex equations with ample notes documented within each method to provide clarification. In addition, parameters could be graphed and modeled visually as well as quickly iterated with matrices and loops.

3.2.2 Excel

Excel was used for calculations and equations not well suited for MATLAB because of their reliance on charts, tables, and figures from outside resources. This includes most calculations based purely off tire data, as well as most structural considerations. Excel allows for the quick manipulation of variable parameters in cells, as well as the side-by-side integration of visual guides and aides.

3.2.3 SolidWorks

SolidWorks 2018 was used for the physical modeling of the suspension in a file SU-93001-BA [16]. The three cardinal planes for design are the ground plane (top), front wheel center plane (front), and car centerline plane (right). According to the SAE axis system, the Z-axis is the vertical direction, the Y-axis is the lateral direction, and the X-axis is the longitudinal direction [2, p. 116]. The planes are show in Figure 6.

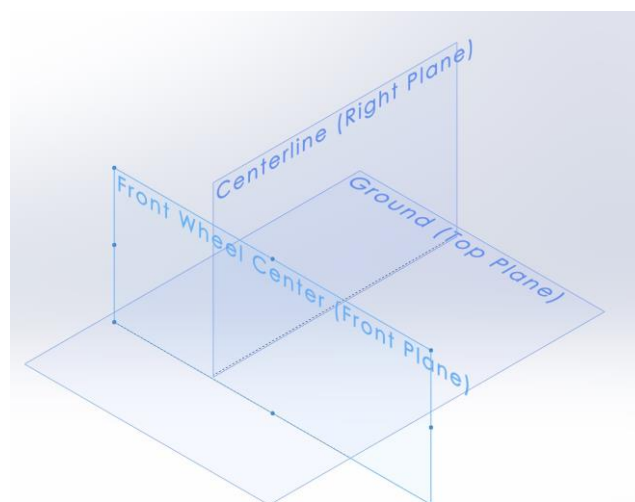


Figure 6: The Cardinal Planes for SU-93001-BA in SolidWorks

In addition to being a sponsor of the FSAE Competition and Wash U Racing, SolidWorks was an ideal choice for modeling the suspension as it allows for complex geometric sketches, 3D layouts and easy adaption to full part models during the design process.

3.2.4 Optimum Kinematics

Optimum Kinematics was used in parallel with SolidWorks during this portion of the process, via the file WashU_Formula_Racing_2019.02Pro [17]. Optimum Kinematics is an industry leading vehicle analysis software used by IndyCar Series, Ferrari, FIA World Endurance Championship, and several Formula One teams, as well as many other divisions of racing and most FSAE teams. The software is laid out with an easy user interface and can quickly produce crucial information about the potential performance of a suspension system. The software uses 4 user-inputted motions: a heave (vertical travel) measured in inches, a roll (lateral angular displacement) measured in degrees, a pitch (longitudinal angular displacement) measured in degrees, and a steer measured in degrees. From these simulation conditions, the software can create plots of important characteristics such as camber gain, motion ratio, roll center migration, and toe variation. These and other inputs will be discussed in more detail below. Figure 7 shows the 2019 front suspension as modeled in Optimum Kinematics.

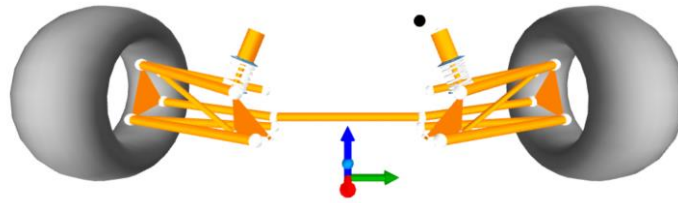


Figure 7: As an example, the 2019 Front Suspension Modeled in Optimum Kinematics

An additional important resource for Optimum Kinematics is the in-depth help file that provides examples and instructions on correctly modeling a given set-up [18].

4 Car and Sensor Data

4.1 Collected Sensor Data

Using the data acquired from the Teksense Sensors and MicroMeasurements sensors, maximum acceleration cases were established for final design of the suspension geometry. Specifically, the team used data from the 3-axis accelerometer to design for peak lateral and longitudinal load transfer cases. The peak values (along with values from other sensors for context of vehicle motion) are show in Table 1.

Run #	A_x [g's]	A_y [g's]	A_z [g's] *note static at -1g	CG Gyro [deg/s]	Front Gyro [deg/s]	Rear Left Travel [mm]	Rear Right Travel [mm]	Engine Speed [rpm]	Front Brake Pressure [psi]	Rear Brake Pressure [psi]	Throttle Position [%]
1	1.84*	-.88	-.62	7.85	15.4	3.76	11.2	4136	268	200	21.3
2	-1.44*	-.106	-.951	-42.3	-23.4	-2.05	-5.82	3371	97.6	95.7	21.8
3	-.883	2.55*	-1.26	-30.8	5.53	3.96	-8.50	--	96.7	95.7	--
4	.052	-2.11*	-.706	12.4	-4.47	-10.4	13.9	--	96.7	93.8	--
5	-.051	1.14	.571*	18.2	28.5	-9.82	2.19	6863	96.7	98.7	36.2
6	-.496	1.08	-3.16*	-4.47	6.02	-.049	-.293	--	96.7	95.7	--

Table 1: The Maximum Values Captured on the Sensor CAN Bus During Fall 2018 Testing

The numbers with asterisks indicate that that is the entry of interest. Values in italics are within a reasonable range of the static value of the sensor. For example, the front brake pressure sensor's static value is around 96.7 psi so any value around that value indicates that the brakes are not in use. Dashed entries mean that the sensor was not operational the time of collection. Most sensors are on different sampling rates and recorded on separate log buses, as a result, some parameters have slightly mismatched timestamps in the raw data.

4.2 Basic Car Weight Parameters – BFR18

As of the technical inspection at the 2018 FSAE Michigan competition, BFR18 had a mass of 294 kg. Using the left-right and front-rear weight distributions, the following matrices were created to quickly evaluate the weight on each side, corner, and axle of the 2018 car. The first matrix is the car's mass in kilograms and the second is the car's weight in pounds.

$$Load = \begin{bmatrix} \textit{Weight on Front Left} & \textit{Weight on Front Axle} & \textit{Weight on Front Right} \\ \textit{Weight on Left Side} & \textit{Total Weight on Car} & \textit{Weight on Right Side} \\ \textit{Weight on Rear Left} & \textit{Weight on Rear Axle} & \textit{Weight on Rear Right} \end{bmatrix}$$

$$\bar{M} = \begin{bmatrix} 70.25 & 139.94 & 69.69 \\ 147.59 & 294.00 & 146.41 \\ 77.34 & 154.06 & 76.72 \end{bmatrix} \text{kg} \quad (1)$$

$$\bar{W} = \begin{bmatrix} 154.88 & 308.52 & 153.64 \\ 325.38 & 648.16 & 322.78 \\ 170.50 & 339.63 & 169.14 \end{bmatrix} \text{lbs} \quad (2)$$

The team expects to reduce weight for the 2019 design year, however, these numbers were used without modification for conservative estimations of new parameters.

In the longitudinal direction, the center of gravity is located a inches behind the front wheel center and b inches in front of the rear wheel center. The weight distribution from Equation 2 can evaluate these parameters. With 47.6% of the weight over the front axle, and a wheel base of 60.5 inches, the distance a from the front wheel center to the center of gravity is 31.7 inches and b is 28.8 inches. Additionally, the center of gravity was found to be 13.56 inches above the ground on BFR18.

BFR18 had a front track width of 46.85 inches and a rear track width of 47.24 inches.

5 Tires and Tire Data

The proprietary tire data is donated by Milliken Research Associates and Calspan TIRF under the FSAE Tire Test Consortium (FSAE TTC) [19]. These data have been crucial to designs across the suspension system to design for max load grip conditions on the tires, as well as understanding ideal alignment conditions. The machine tests tires in straight-line driving/braking conditions as well as cornering and high lateral force situations. Using a sandpaper mat and universal spindle, the machine measures hundreds of tire parameters such as pneumatic trail, lateral force, longitudinal force, slip angle, among others at different pressures, velocities, loaded radii, normal forces, and camber angles.

5.1 Tire Selection

For many years, while using 13" wheels, Wash U Racing used two different tires for the front and rear of the car. The front had Hoosier R25B compound 20.5x7.0-13 and the rear used Hoosier

R25B compound 20.0x7.5-13 tires. As with consumer cars, staggered tires should only be used in cases of severe weight imbalance between the front and rear axles. Additionally, if the car is desperately struggling for grip due to poor camber or toe alignment, wider offset tires could be used to compensate for lacking performance [20, pp. 56-57]. As a result of the BFR18's weight balance of roughly 48% front and 52% rear, the tires should not be staggered. As of the most recent round of FSAE TTC testing in August of 2018, there were 7 Hoosier tires in contention for WUFR-19 as presented in Table 2.

Dimensions	Compound	Item Number	Approximate Weight	Price
18.0x6.0-10	R25B	43101	9lbs	\$140.80
18.0x7.5-10	R25B	43105	10lbs	\$156.00
16.0x6.0-10	R25B	43070	7lbs	\$140.80
16.0x7.5-10	R25B	43075	8lbs	\$156.00
6.0/18.0-10	LCO C2000	41100	8lbs	\$159.00
6.0/16.0-10	LCO C2000	43070	7lbs	\$140.80
7.5/16.0-10	LCO C2000	43075	8lbs	\$156.00
20.0x7.5-13	R25B	43168	12	\$192.20
20.5x7.0-13	R25B	43163	11	\$179.20

Table 2: The Available Hoosier Tires for the 2019 Design Year [21]

Due to limitations of the testing machine, all 16" outer diameter tires could not be tested on the Calspan TIRF machine under drive/brake conditions (only free rolling cornering) [22]. As a result, teams were encouraged to create their own testing protocols for these tires, however, Wash U Racing selected tires that had been tested in all circumstances by the consortium. After comparing data in OptimumTire for the remaining 3 tires (2 R25B and 1 LCO), the Hoosier R25B 18x7.5-10 tires were selected for all four wheels of WUFR-19. Through tire selection alone the team will be cutting approximately 6lbs of unsprung weight.

5.2 Tire Data

FSAE TTC data provided crucial data for the design of the suspension and steering system. Specifically, the data was used for analysis of pressure, spring rate, friction, slip angle, aligning torque, lateral force, longitudinal force, and normal force. Slip angle, cornering stiffness, and aligning torque will be discussed here and were used for analysis. Note that all parameters are evaluated as the absolute value as different models and axis systems define directions differently – the crucial elements are the magnitude and trends. All of the data represented in Figure 9, Figure 10, Figure 11, and Figure 13 from the FSAE TTC have been de-identified. As per the team's user agreement with Calspan, the key and axis values have been removed from the charts for publication. They can be found in their entirety in internal team documents. Additionally, the tire fitment model used in OptimumTire was the Pacejka Magic Formula 2006. The reason for the selection of this model is not within the scope of this report.

The unifying theory behind each of these characteristics of the tire is the slip angle. Figure 8 shows a view of a tire slip angle from the road's perspective.

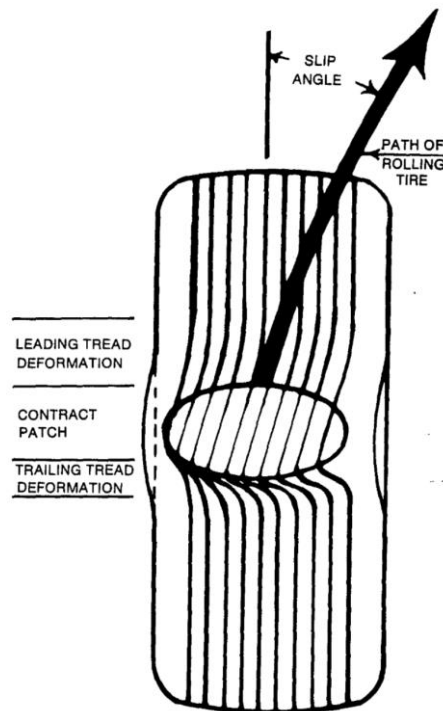


Figure 8: The Definition of a Tire Slip Angle [1, p. 14]

Because tires are highly elastic material with coefficients of friction above 1, the tread will grab the ground and stretch as the car moves. The coefficient of friction for a tire is given by Equation 3 [1, p. 26]:

$$\mu = \frac{F_y}{F_z} \tag{3}$$

Where μ is the coefficient of friction [unitless], F_y is the lateral force [lbs], and F_z is the normal force [lbs]. The coefficient of friction can also be related in terms of acceleration when mass is constant, through Newton's Second Law For example, from Table 1 - Run 4, the coefficient of friction is:

$$\mu = \frac{2.11 g}{.706 g} = 2.98$$

These data can also be found from the tire data from the TTC, however this is a calculation from Wash U Racing's collected data.

In the longitudinal direction, this helps the tire gain traction on launch and under acceleration. In the lateral direction, it maintains grip while also causing inefficiency during turning. This is because the tire rotates under steering input from the driver, however the tire tread grabs the ground and lags behind the intended heading of the tire. If this effect is too great, the driver will not be able to assess the true direction of the tires and the car will have unmanageable understeer.

Figure 9 shows a plot of lateral force against slip angle. This graph is structured similar to the stress-strain curve of any elastic material. In the linear section, the tire is controllable and

deforming a known, predictable amount. When the curve peaks and flattens out, the tire has “broken free” of its grip, lost traction, and begun to slip [2, p. 25].

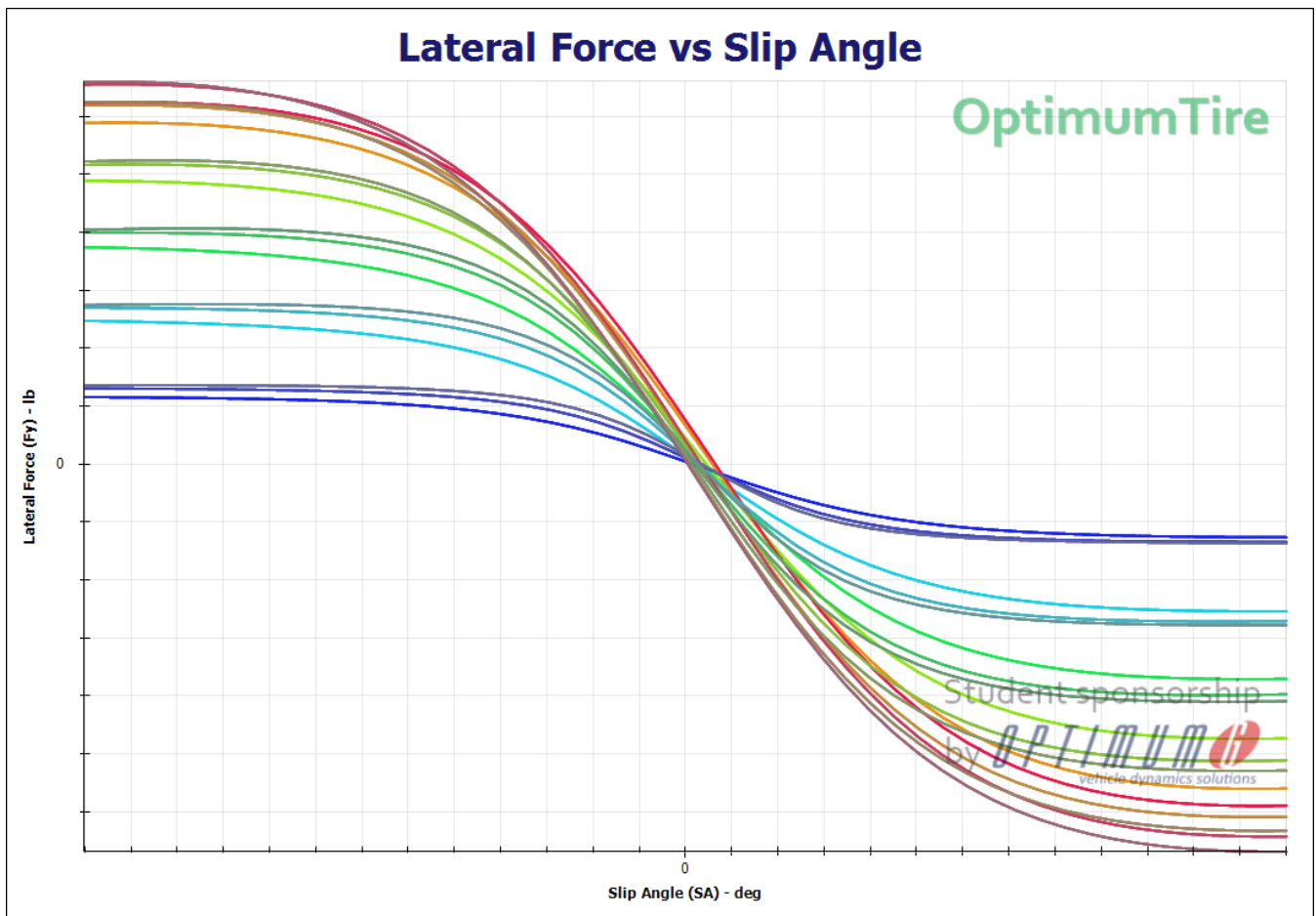


Figure 9: The De-Identified Graph of Lateral Force Against Slip Angle for the R25B 18.0x7.5-10 [23]

Lateral force is the force exerted on the tire, perpendicular to its direction of travel, by the road as the wheel is steered. This force deforms the tire normal to its direction of motion causing the slip angle deformation. It is dependent on the normal force on the tire and the camber angle of the tire. Unlike common street radial tires, Hoosier R25B 18.0x7.5-10's are cross-ply tires. This means that they do not have a steel core, but rather a nylon core and very little sidewall support [13, p. 1]. As a result, they are very sensitive to camber change (it was determined from these data that most attributes besides spring rate are independent of pressure). Figure 9 shows the extensive dependency on angle and load for this tire. A large design constraint for the suspension system was ensuring constant load on each corner and low camber angle through all motions. This is accomplished through even roll resistance, well designed anti-roll geometry, and properly modeled camber curves.

Looking only at the graph of lateral force against slip angle, it is clear that tires with less camber and high normal force will have the most grip before slipping, however, cornering stiffness must be considered before judgements are made about maximum grip conditions. Figure 10 and Figure 11 show the relation between cornering stiffness and lateral force, as well as cornering stiffness and slip angle. As lateral force increases, cornering stiffness generally increases (as shown in Figure 10). In Figure 11, however, the slip angle decreases as the cornering stiffness increases.

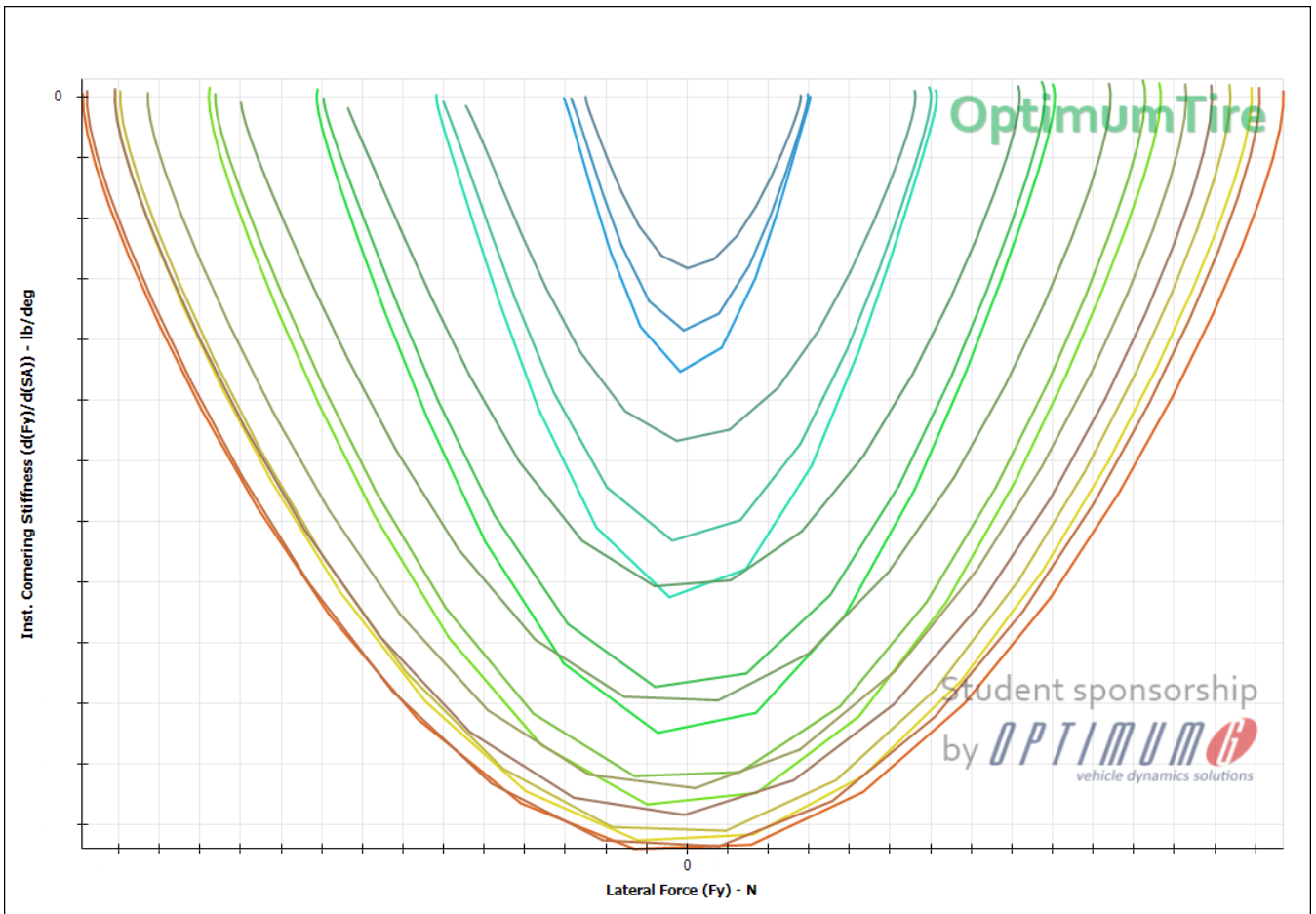


Figure 10: The De-Identified Graph of Instantaneous Cornering Stiffness Against Lateral Force for the R25B 18.0x7.5-10 [23]

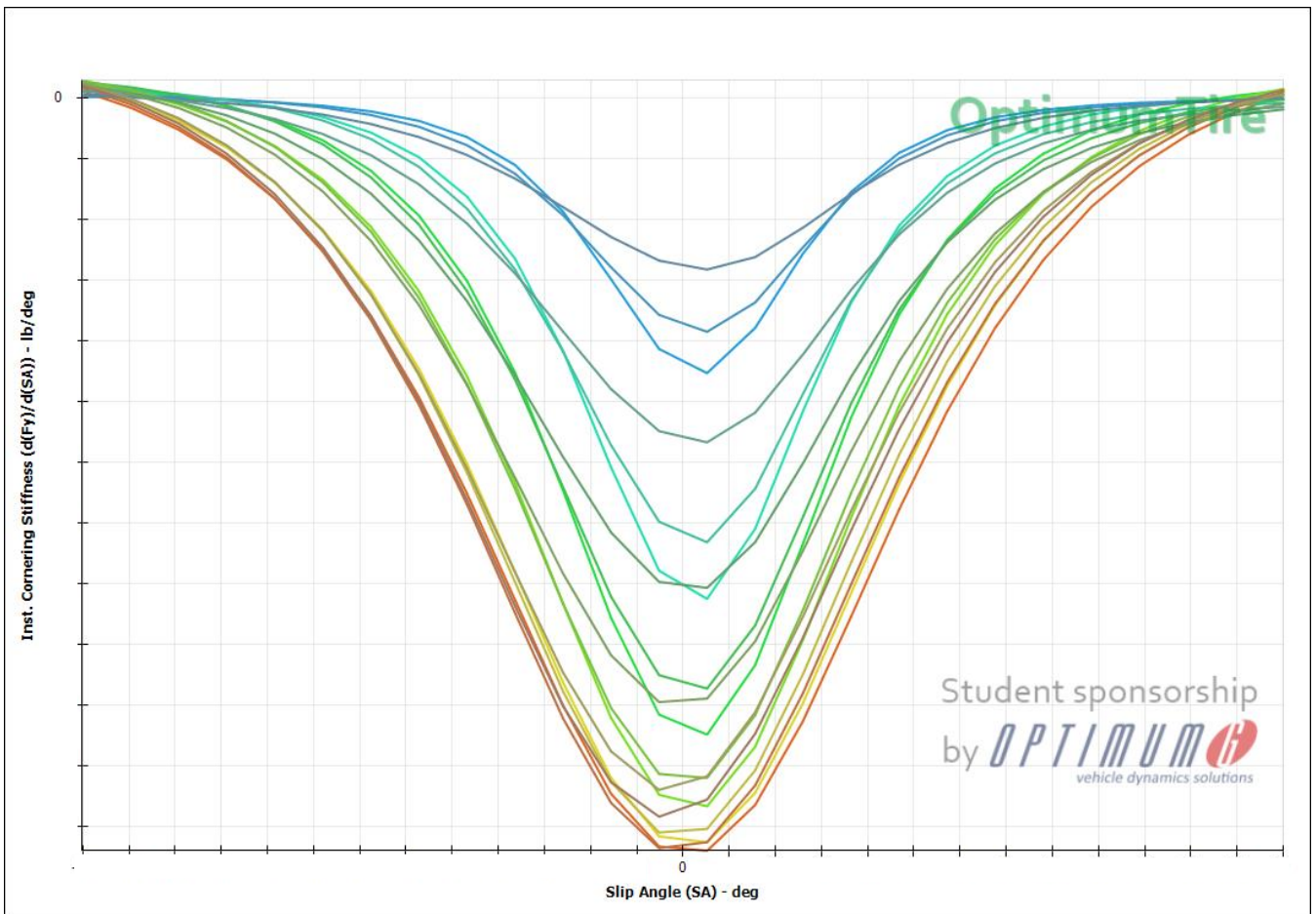


Figure 11: The De-Identified Graph of Instantaneous Cornering Stiffness Against Slip Angle for the R25B 18.0x7.5-10 [23]

Cornering stiffness is defined in Equation 4:

$$C = \frac{dF_y}{dSA} \quad (4)$$

Where C is the cornering stiffness [lbs/deg], F_y is the lateral force [lbs], SA is the slip angle [deg], and the entire equation is a function of F_z (normal force [lbs]) and γ (inclination angle [deg]). The racing tire is a pressure vessel and as the load on the tire increases, it becomes stiffer (cornering stiffness goes up). This causes the slip angle to go down. As a result, pure increases in lateral force do not drag the tire so much that it is unusable, but instead it is balanced as load is transferred. This is an important consideration when designing anti-roll geometry as a lighter loaded tire will slip less by Figure 9, while a heavier loaded tire will slip less by Figure 11.

The final integral tire graph is aligning torque against slip angle as shown in Figure 13. Aligning torque is the resistance felt by the driver as they steer the wheel. It is the pneumatic trail (intrinsic offset of the applied lateral force compared to the centerline of the wheel in the transverse plane) times the lateral force applied to the tire.

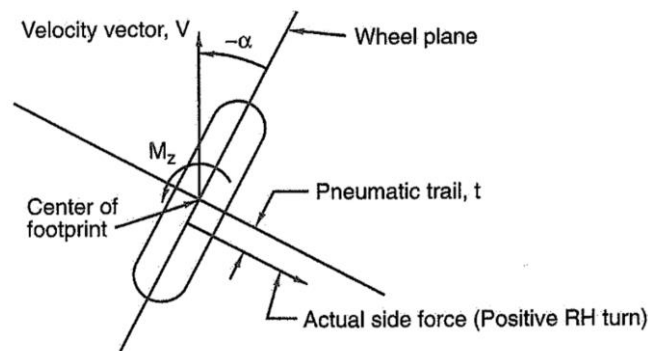


Figure 12: Aligning Torque on the Footprint of a Tire [2, p. 70]

The trail value changes as the tire is turned, causing the aligning torque to increase until a peak then sharp drop off. This increase is the resistance the driver feels as the tires approach sliding before losing traction. The designer should incorporate some scrub radius (offset between ball joint axis and contact patch in the front view) and mechanical trail (offset between ball joint axis and contact patch in the side view) for the driver to have this feel, if not, they will not know when the tires approach sliding [1, p. 21]. These effects are only felt at low speeds as they are overwhelmed by pneumatic trail at high speeds.

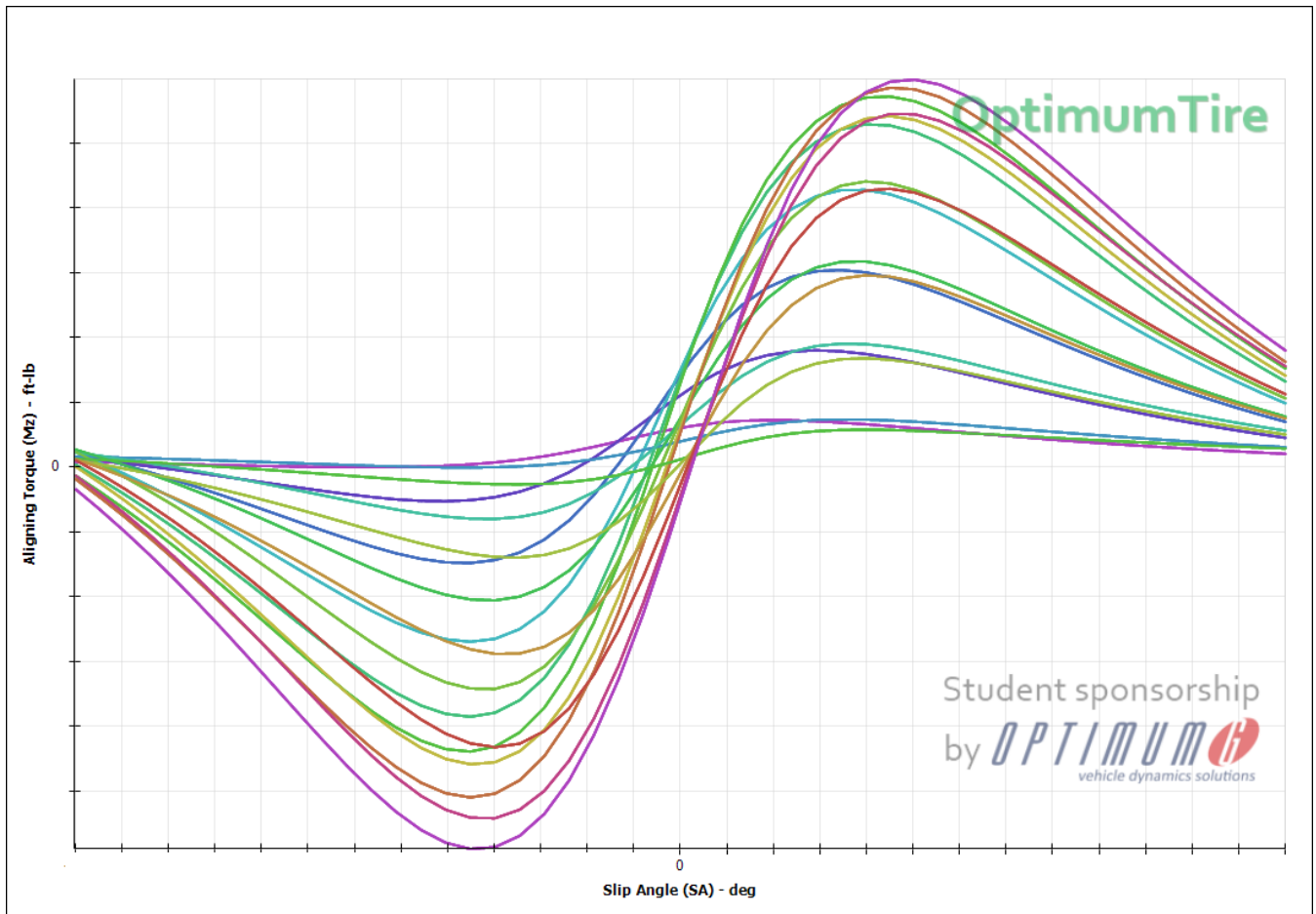


Figure 13: The De-Identified Graph of Aligning Torque Against Slip Angle for the R25B 18.0x7.5-10 [23]

As lateral force, cornering stiffness, and slip angles are calculated, they should be compared back to this graph to ensure that the maximum values do not exceed breakaway for reasonable steering inputs from the driver. These conditions should all be considered to meet the team goal of drivability and driver control.

5.3 Application of Tire Data

The first main suspension geometry calculation dependent on tire data (besides ride height) is lateral force calculations to ensure that the correct tire compound and dimensions are selected. There are two methods for solving for the slip angle of the tires, in conjunction with Figure 9 - Figure 15. The system is split in longitudinal halves using a bicycle model from Figure 14.

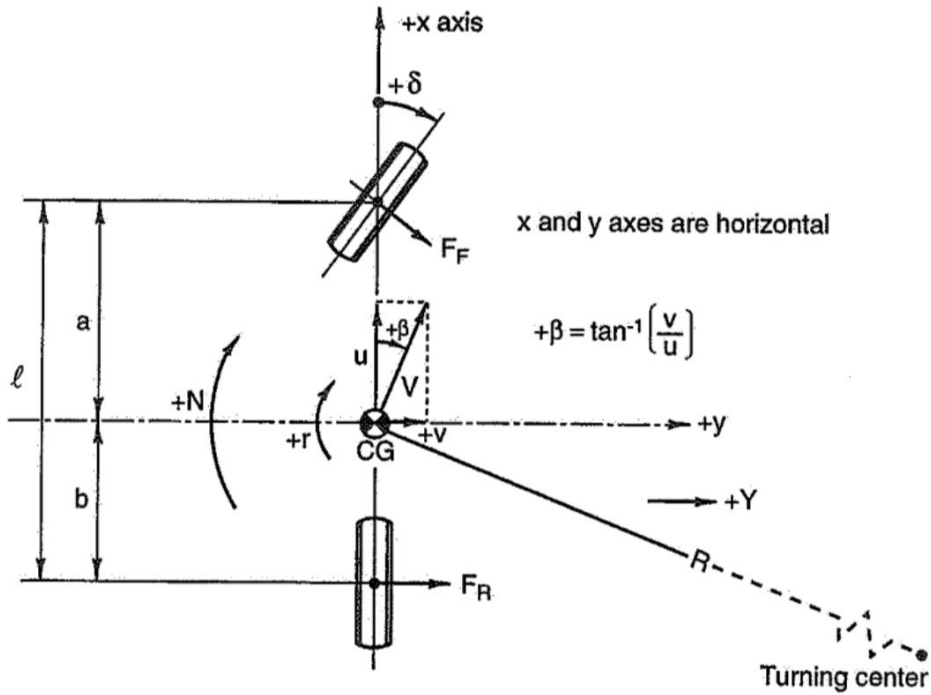


Figure 14: The Bicycle Model [2, p. 127]

The equation for total lateral force in a bicycle model system is presented in Equations 5a , 5b, and 5c:

$$Y_F = C_F \beta + C_F \left(\frac{ar}{V} \right) - C_F \delta \quad (5a)$$

$$Y_R = C_R \beta - C_R \left(\frac{br}{V} \right) - C_R \delta \quad (5b)$$

$$Y = Y_F + Y_R \quad (5c)$$

Where Y is the total lateral force [lbs], Y_F is the front lateral force [lbs], Y_R is the rear lateral force [lbs], C_n is the cornering stiffness for a given front or rear tire [lbs/rad], β is the total vehicle slip angle [rad], a is the distance from the front wheel center to the center of gravity [in], r is the yawing velocity of the vehicle [1/sec], V is the total vehicle speed [ft/sec], δ is the wheel steer angle [rad], and b is the distance from the rear wheel center to the center of gravity [in] [19, p. 149].

Additionally, the equation will be rearranged and evaluated as Cornering Stiffness in Equations 5d and 5e:

$$C_F = \frac{Y_F}{\beta + \frac{ar}{V} - \delta} \quad (5d)$$

$$C_R = \frac{Y_R}{\beta - \frac{br}{V} - \delta} \quad (5e)$$

The values of lateral force, vehicle slip angle, center of gravity position, vehicle velocity, and wheel turn angle are either set by parameter or determined from a graph. Yaw velocity, however, must be solved for using Equation 6:

$$r = \frac{R_w \omega_i}{R_1 - \frac{w_r}{2}} \quad (6)$$

Where r is the yaw velocity [1/sec], R_w is the radius of a wheel [feet], ω_i is the angular velocity of the rear inner wheel [1/sec], R_1 is the radius of rotation of the center of the rear wheels [ft], and w_r is the rear track width [ft] [11, p. 400]. Table 3 shows the evaluated values for yaw velocity.

R_w	ω_i	R_1	w_r	r
0.7625 ft	$37.38 \frac{1}{sec}$	28.04 ft	3.96 ft	$1.094 \frac{1}{sec}$

Table 3: The Yaw Velocity for WUFR-19

The parameters are in Table 4 for a simulated left turn assumed 50/50 front-rear weight balance:

β	a	b	$\delta_{FrontLeft}$	$\delta_{FrontRight}$	$\delta_{RearBoth}$	r	V
6 deg	30.25 in	30.25 in	33 deg	25 deg	0 deg	$1.094 \frac{1}{sec}$	19.4 mph
.105 rad	2.52 ft	2.52 ft	.576 rad	.436 rad	0 rad	$1.094 \frac{1}{sec}$	$28.5 \frac{ft}{s}$

Table 4: The Parameters for Lateral Force and Cornering Stiffness Calculations

Moreover, the simulated left turn will induce 1.2g's of later acceleration and no longitudinal acceleration as shown in a modified weight matrix:

$$W_{LeftTurn} = \begin{bmatrix} 59.03 & 325 & 265.97 \\ 105.23 & 650 & 544.77 \\ 46.20 & 325 & 278.80 \end{bmatrix} lbs$$

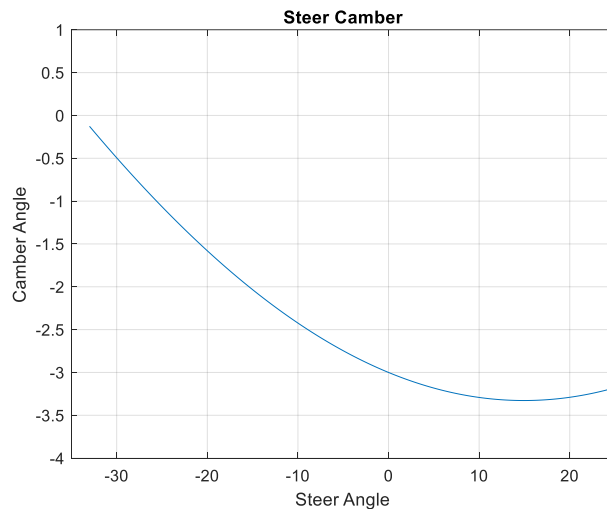


Figure 15: The Steer Camber Curve for the 1.2g Left Turn

The peak steer camber values from Figure 15, produces transient camber values at max steering lock in Table 5:

	Left	Right
Front	-0.127 deg	-3.178
Rear	-2 deg	-2 deg

Table 5: Camber Values for Max Steering Lock for a Left Turn with 1.2g's of Lateral Acceleration

Evaluation begins with Figure 9, and the max lateral load capacity for each wheel. If the lateral force here is exceeded, the wheel will lose traction and (on the inside wheel) cause an oversteer response or (on the outside wheel) an understeer response. From the weight matrix and Table 5, the max loads can be determined in Table 6:

	Left	Right
Front	130 lbs (578.27) N	650 lbs (2891.34) N
Rear	130 lbs (578.27) N	650 lbs (2891.34) N

Table 6: The Maximum Lateral Force Capability of Each Tire Under Steer

The normal loads were approximated to match the domain entries on the tire data graphs. From here, cornering stiffness values were calculated for each corner under the turn condition in Table 7:

	Left	Right
Front	7.05 lbs/deg	56.3 lbs/deg
Rear	37.40 lbs/deg	71.92 lbs/deg

Table 7: The Cornering Stiffness Values for Each Tire in Steer

The next step is to evaluate Figure 10 to ensure that the value of cornering stiffness is appropriate for the same lateral force. Tracing both axes to the respective curves on the graph of Instantaneous Corning Stiffness against Lateral Force, all of these values fit their respective curves after some iteration of vehicle slip angle and lateral force. These calculations can be found in the document: Lateral Force Calculator.xlsx [24]. From there, the cornering stiffness can be moved to Figure 11 and traced down on the respective normal force/camber curve to a slip angle. Without an anti-roll bar or any load controlling condition, the slip angles are presented in Table 8

	Left	Right
Front	3 deg	5 deg
Rear	5 deg	5.5 deg

Table 8: The Slip Angles for the 1.2g Left Turn

Finally, the slip angles are compared on Figure 13 and back on Figure 9 to ensure that the tires would not slip under the angles and loading. From here, steering geometry can be developed, and tire selection can be finalized. This is not an exhaustive array of calculations based on tire data, however, it is an important starting point for eliminating tire choices that do not provide suitable grip.

6 Suspension Geometry

As discussed above, the role of the suspension is to guide the motion of the chassis and control the contact patch of the tire against the ground. With those constraints in mind, the WUFR-19 geometry has two main sections with two distinct considerations. The first, more theoretical part of the geometry is concerned with the wheel motion and contact on the ground and is encompassed in the front and side view geometries. The second is housed in the push/pull alignment of the spring-damper system. Most results from simulations and figures from SolidWorks will focus on the front suspension geometry as it is more complicated to create. Many parameters crucial for steering and driver control are not present in the rear setup.

6.1 Front View Geometry

6.1.1 Wheelbase

As referenced in rule T.1.2.1, the car must have a wheelbase of at least 1525mm (60.04 inches) to pass technical inspection. For the WUFR19, the team selected a wheelbase of 1537mm (60.50 inches) to ensure that manufacturing tolerance in frame welding and final assembly would not cause a rules violation. This is shown in SU-93001-BA in Figure 16.



Figure 16: The Front and Rear Wheel Center Planes Set a Distance Apart by the Wheelbase

A longer wheelbase provides for better longitudinal load transfer characteristics under braking, more room for ergonomic comfort for the driver and generally easier packaging. However, using the shortest legal wheelbase reduces weight and still leaves room to achieve the same control under braking, driver comfort, and component fitment with more work.

6.1.2 Longitudinal Load Transfer

In all cases the longitudinal acceleration due to braking should be larger than that of straight-line acceleration. As a result, the peak braking acceleration of 1.84 g's in the positive x-direction from Table 1 was used for all calculations. Longitudinal Load Transfer was calculated using Equation 7 from Tune to Win [1, p. 32]:

$$LT_{long} = a_{long} * \frac{W}{\ell} * h \quad (7)$$

Where LT_{long} is the longitudinal load transfer [lbs], a_{long} is the peak acceleration [g's], W is the weight of the car [lbs], ℓ is the wheelbase [in], and h is the height of the center of gravity [in] [1, p.

32]. Using the value $\overline{W}_{2,2}$ from Equation 2, the acceleration collected from the sensor array, the wheelbase determined in the previous section, and a previously measured center of gravity height from internal team documents, the forward longitudinal load transfer under braking is:

$$1.84g * 648.16 \text{ lbs} * \frac{13.56 \text{ in}}{60.5 \text{ in}} = 267.30 \text{ lbs}$$

This weight transfer is assumed to be shared equally between the left and right rear wheels and thus the new weight matrix under peak brake loading is given by the following:

$$\overline{W}_{braking} = \begin{bmatrix} 288.53 & 575.82 & 287.29 \\ 325.38 & 648.16 & 322.78 \\ 36.85 & 72.33 & 35.48 \end{bmatrix} \text{ lbs}$$

Heavy braking results in a substantial amount of weight moving from the rear tires to the front tires. Using the values a and b for the longitudinal center of gravity calculated in the previous section, the maximum load transfer, and the softest rate (most conservative) spring found in Appendix A.1, this weight transfer can be related to a pitch angle of the car under braking by Equation 8:

$$\theta_{front} = \tan^{-1}\left(\frac{LT_{long}}{2 * K_s * a}\right) \quad (8)$$

Where θ is the pitch angle of the car [deg], LT_{long} is the longitudinal load transfer under braking [g's], $K_s(\text{low})$ is the softest spring rate usable on the car [lbs/in], and a is the distance between the center of gravity and the front wheel center. Using a 150 lbs/in spring, this evaluates to 1.60 degrees of forward pitch angle under maximum braking. This value was carried in to the OptimumKinematics pitch motion for analysis of camber, toe, and pitch center variation. Figure 17 shows the plot of pitch angle for analysis.

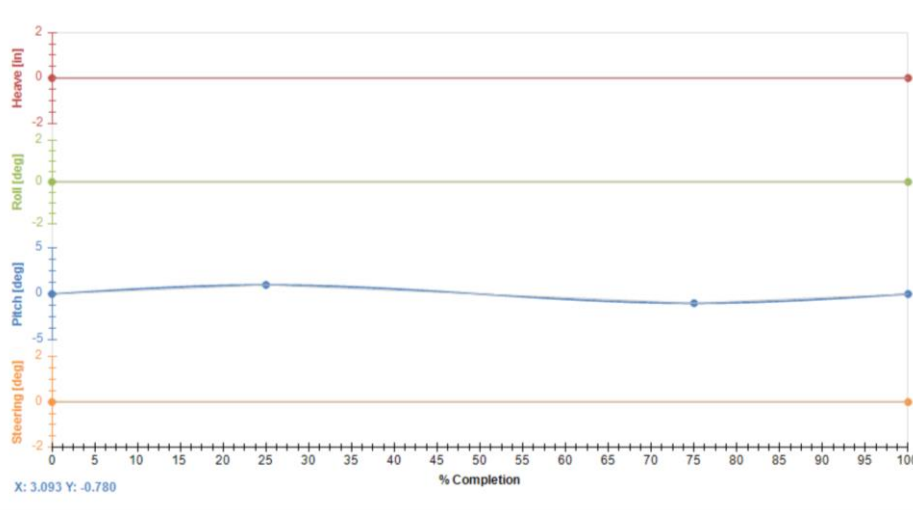


Figure 17: The Pitch Motion Loaded in to OptimumKinematics

The final consideration in the longitudinal direction are “anti” geometries. Anti-dive and anti-squat geometry allow for the control arms to mitigate pitch displacement of the sprung mass by loading these components. In the side view, one bushing for a given control arm must be out of plane with the other to achieve this geometry [2, p. 617]. If the front upper control arm is angled downward, the car will resist dive under braking. If the rear upper control arm is angled upward, the car will resist squat in acceleration. These geometries are more important for a car using an

aerodynamics package (notably a front wing with low clearance). To avoid putting control arms in bending, this geometry was not considered.

6.1.4 Track Width

As a racecar travels through a turn, weight is moved from the inside wheel to the outside wheel in an overturning motion that attempts to flip the car away from the apex center of the turn. This is known as lateral load transfer and a good suspension geometry will limit its impact on performance and speed. As shown in the tire graphs in Section 4, severe weight transfer will unload the inside tire causing washout oversteer as the driver suddenly spins in to the turn. On the flip side, if not enough load is transferred to the outside tire during a turn, the guiding tire will not have enough grip to sufficiently steer the car and an understeer effect will be introduced. Severe oversteer may result in a spin while understeer will result in decreased performance – both are to be avoided for optimal racing. Equation 9a solves for lateral load transfer:

$$LT_{lat} = a_{lat} * W_n * \frac{h}{t_n} \quad (9a)$$

Where LT_{lat} is the lateral load transfer [lbs], a_{lat} is the lateral acceleration [g's], W_n is the weight of the given axle (front or rear) [lbs], h is the height of the center of gravity [in], and t_n is the track width of a given axle (front or rear) [in] [2, p. 679].

Additionally, lateral acceleration will be calculated using the relationship in Equation 10:

$$a_{lat} = \frac{V^2}{R} \quad (10)$$

Where a_{lat} is the lateral acceleration [g's], V is the velocity of the car [ft/sec], and R is the radius of a turn measured from the center of gravity of the vehicle to the center of the corner's apex [ft].

Three methods were considered for calculating the minimum required trackwidth using lateral load transfer: setting a target time on the skid pad event and calculating subsequent transfer, applying the rules required for lateral stability, and considering the tightest turn radius that the car must be able to achieve by rules. However, before trackwidth can be completely solved for, the variables for lateral load transfer and center of gravity height must be eliminated.

The first method for calculating the minimum trackwidth from lateral load transfer was to look at the BFR18's best Skidpad performance at FSAE Michigan 2018. Specifically, the best run of the day produced a time of 6.182 seconds around the track from Figure 3. This time placed the team in position 55/99 teams that participated in the event. If the team wants to place in the top 30 teams in this event in 2019, a target time of 5.852 seconds was set.

Using half of BFR18's trackwidth (to get the center of the car's travel) and the inside radius of the Skidpad from Figure 3, and assuming a constant velocity around the track, BFR18's actual and target speeds were found. The assumption of constant velocity was not correct, however, due to lack of data, the assumption was made that on the second loop around the Skidpad, the car would perform at a near constant speed. Table 3 shows the resulting acceleration and lateral load values for the actual and target times around the Skidpad track [15].

Time [s]	Acceleration [g's]	Front LT_{lat_1} [lbs]	Rear LT_{lat_1} [lbs]
6.182 (actual)	1.0164	90.725	99.042
5.852 (target)	1.0737	95.842	104.63

Table 9: The Lateral Acceleration and Load Transfer Using the Target Time Method

Assuming a left turn, this produces an altered weight matrix:

$$\overline{W}_{Lat_1} = \begin{bmatrix} 64.15 & 308.52 & 244.37 \\ 156.80 & 648.16 & 509.35 \\ 92.65 & 339.63 & 264.98 \end{bmatrix} lbs$$

The second method for solving for trackwidth comes from rule IN.9.2.2 which says, "The vehicle does not roll when tilted at an angle of 60 degrees to the horizontal, corresponding to 1.7g," [3, p. 104]. Once again solving Equation 7, now using 1.7g's of lateral acceleration, Table 4 produces the values:

	LT_{lat_2} [lbs]
Front	151.75
Rear	165.66

Table 10: The Lateral Load Transfer on the Inspection Tilt Test

As a result, on a left turn this produces a weight matrix:

$$\overline{W}_{Lat_2} = \begin{bmatrix} 3.13 & 308.52 & 305.39 \\ 7.97 & 648.16 & 640.18 \\ 4.84 & 339.63 & 334.79 \end{bmatrix}$$

This is very close to the upper limit for control of the car as the inside tire is almost entirely unloaded and could washout during an event.

For the third method, a peak performance turn was considered. In rule D11.2.2.d, the minimum hairpin outer diameter is listed as 9m [3, p. 126]. Additionally, in D11.2.2.g, the track is listed as 4.5m wide [3, p. 126]. Removing a halftrack and some distance between the maximum outer radius and the width of the track, a turn of 10ft (3.04m) was decided upon with an acceleration of 1.8g's. The resultant lateral load transfers can be found in Table 11.

	LT_{lat_3} [lbs]
Front	160.68
Rear	175.4

Table 11: The Lateral Load Transfer for the Third Method of Taking a High Speed Hairpin Turn

As a result, the adjusted weight matrix is

$$\overline{W}_{Lat_3} = \begin{bmatrix} -5.8 = 0 & 308.52 & 308.52 \\ -10.7 = 0 & 648.16 & 648.16 \\ -4.9 = 0 & 339.63 & 339.63 \end{bmatrix} lbs$$

This intensity of a turn would not be handled by the BFR18 suspension setup, therefore the WUFR19 geometry must be amended to withstand this loading. Because weight is set by the entire team and not just the suspension system, there are two independent variables that can be changed to achieve this grip: the trackwidth and the center of gravity height. Rearranging Equation 9a, the center of gravity can be solved for as:

$$h = LT_{lat} * \frac{t}{W * a_{lat}} \quad (9b)$$

Just as with the lateral load transfer, the maximum center of gravity height must be considered for multiple load cases and with two different axle dependencies. First, a lateral load transfer has to be determined. For BFR18 values, all load is assumed to transfer across the car. The maximum allowable center of gravity height due to tilt test with front and rear axle dependencies will be calculated, followed by the maximum allowable due to the 1.8g applied turn. Table 6 shows the maximum center of gravity heights for different acceleration and loading conditions.

	Front Lateral Load Transfer [lbs]	BFR18 Front Track [in]	Rear Lateral Load Transfer [lbs]	BFR18 Rear Track [in]	h with front dependency [in]	h with rear dependency [in]
1.7g Tilt Test	154.88	46.85	170.50	47.24	<u>13.83</u>	<u>13.95</u>
1.8g Applied Turn	154.88	46.85	170.50	47.24	<u>13.07</u>	<u>13.18</u>

Table 12: The Maximum Center of Gravity Height for Different Load Conditions

A center of gravity height of 12 inches will be used for calculations on the WUFR-19. To accommodate this, the 2019 front and rear track will increase, and several component changes on the car will work to lower the center of gravity. Specifically, the engine is moving down 1 inch relative to the frame, the wheels are being downsized, and several power train components including the exhaust are moving closer to the ground.

The next and final step is to determine the track width using another variant of Equation 9a:

$$t_n = \frac{h * W_n * a_{lat}}{LT_{lat}} \quad (9c)$$

Using the Lateral Force and Slip Angle graph from Figure 8, it can be seen that unloading the inside tire too much can cause the car to slide into oversteer. For WUFR-19, the system was designed for 20lbs of normal load to remain on the unloaded front tire for the tilt test and 15lbs to remain on the rear inside tire for the applied load turn. With load transfer determined, as well as center of gravity height, and peak acceleration, minimum track width values for the front and rear can be determined. Table 7 shows the minimum track width for the front and rear given the load conditions and center of gravity heights.

	Front Lateral Load Transfer [lbs]	Center of Gravity Height [in]	Rear Lateral Load Transfer [lbs]	Front Track Width [in]	Rear Track Width [in]
1.7g Tilt Test	134.88	12	150.50	<u>46.66</u>	<u>46.04</u>
1.8g Applied Turn	139.88	12	155.50	<u>47.64</u>	<u>47.18</u>

Table 13: The Minimum Required Trackwidth for the Desired Load Transfer with the Calculated Center of Gravity Height

To accommodate for errors in calculation, the track width in the front will be 48.5 inches and the rear track will be 47.5 inches. The track width values are staggered for drivability. Because WUFR-19 will not have a front wing, the inside front tire will be the only marker to avoid cones around corners. If the front and rear tracks are staggered, the driver can aim for the front tire to avoid a cone and be sure that the rear tire also avoids that cone. If the rear track is wider, the front tire could miss the cone and the rear tire could hit the cone. Figure 18 shows the track planes on SU-93001-BA.

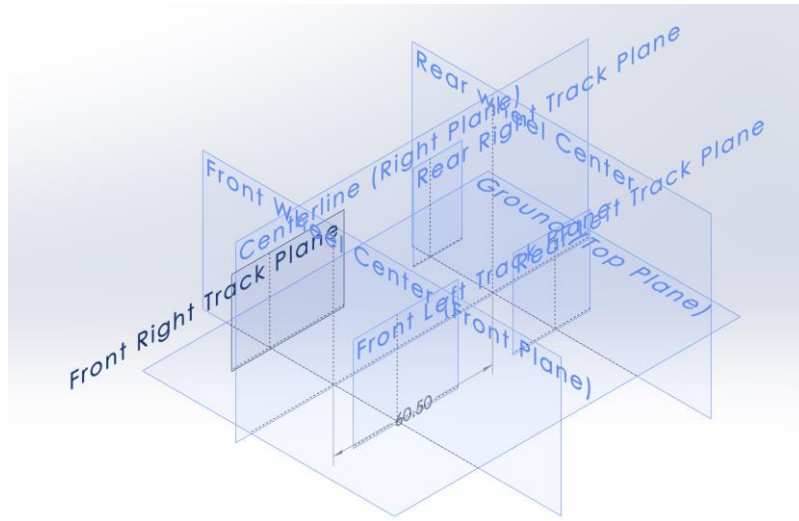


Figure 18: SU-93001-BA with Front and Rear Track Planes on Both Sides of the Car

6.1.5 Roll Center Heights

The next step in building a suspension geometry is setting the front and rear roll center heights. When lateral force is applied through the tires, it is reacted by the center of gravity of the car. The roll center (and its position relative to the ground and the center of gravity) determines the magnitude of the rolling and nonrolling overturning moments [1, pp. 29-30]. The rolling moment is the force applied at a distance between the center of gravity and the roll center – it must be reacted by the springs [2, p. 614]. The nonrolling overturning moment is the force times distance between the roll center and the ground that must be reacted by the stiffness of the chassis, thus it is said that the position in the z-direction of is a tradeoff [2, p. 614].

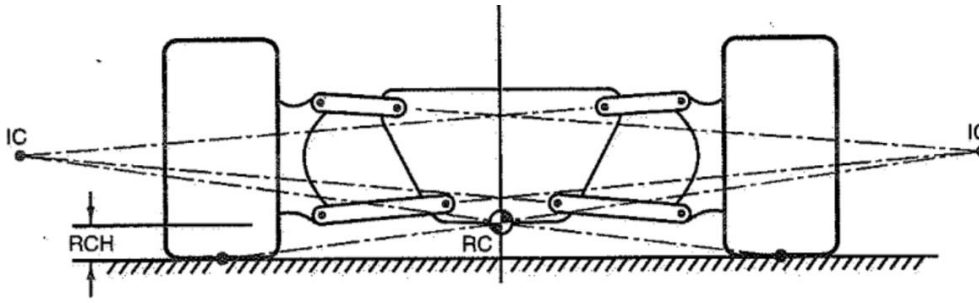


Figure 19: A Roll Center Height on a Suspension Geometry [2, p. 614]

If a roll center is too high, it will induce a jacking effect on each corner. In jacking, a lateral force put through the tire is reacted with a vertical component that pushes the unsprung wheel upwards instead of applying the desired tension-compression through the control arm linkages [2, p. 38].

BFR18 and several previous Wash U Racing cars had a front roll center above the rear roll center. This resulted in a roll axis (the line between the centers) that was raked upwards from rear to front. As a result, the car resisted its own rolling moment through the axis, decreasing drivability. The roll center heights were established through roll rate calculations presented in chapter 16 of Race Car Vehicle Dynamics [2, p. 585]. These calculations were iterated until proper heights were found. These calculations can be found in the team's MATLAB file [15]. First, Equation 10 shows the force applied to the center of gravity in a turn.

$$F_{cg} = m_{sprung} * a_{lateral} \quad (10)$$

Where F_{cg} is the force enacted on the center of gravity [lbs], m_{sprung} is the sprung mass of the car [slugs], and $a_{lateral}$ is the lateral acceleration [g's]. Note that this method neglects tire grip and capabilities focusing instead on the geometry.

The rolling and nonrolling moment arms were taken by subtracting the height of each roll center from the height of the center of gravity and the distance from the ground, respectively. Equations 11 and 12 calculate the rolling and nonrolling moments:

$$M_{rolling} = F_{cg} * x_{rolling} \quad (11)$$

$$M_{nonrolling} = F_{cg} * x_{nonrolling} \quad (12)$$

Where $M_{rolling}$ is the rolling moment [lbs*in], $M_{nonrolling}$ is the nonrolling moment [lbs*in], F_{cg} is the force applied to the center of gravity [lbs], $x_{rolling}$ is the distance between the center of gravity and the roll center [in], and $x_{nonrolling}$ is the distance between the roll center and the ground [in].

Table 8 shows the final roll center heights, along with the accompanying rolling and nonrolling moments associated with each center.

	Height [in]	Rolling Moment [lbs*in]	Nonrolling Moment [lbs*in]
Front Roll Center	1.5	3224.04	460.58
Rear Roll Center	2.25	2993.76	690.88

Table 14: The Roll Center Heights with Rolling and Nonrolling Moments

In the front view suspension geometry, the tire contact point on the ground is connected to the suspension instantaneous center through the roll center. To complete this line, the front view swing arm must be established by considering camber curves.

6.1.6 Front View Swing Arm Length

The front view swing arm (FVSA) positions the instantaneous center of the suspension in relation to the tire contact point.

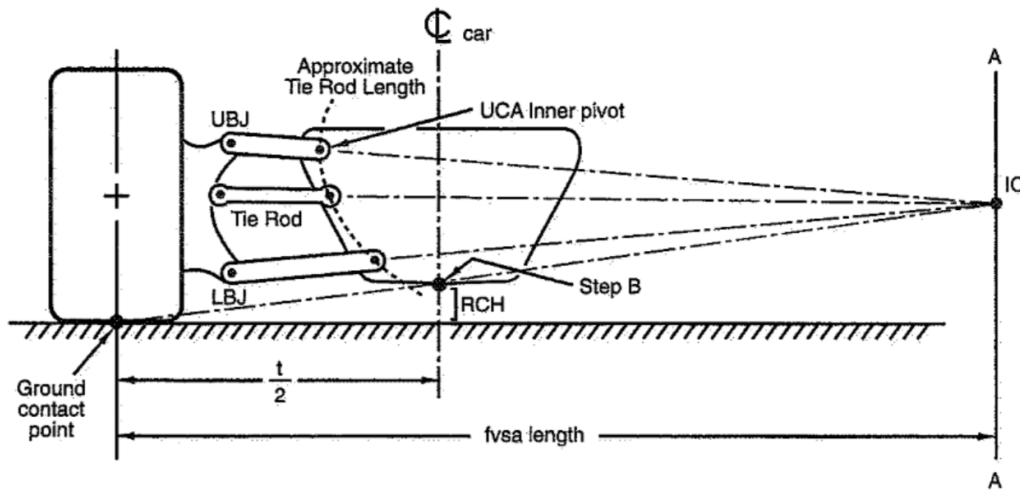


Figure 20: The Front View Swing Arm [2, p. 628]

After the FVSA is determined, all suspension linkages are traced out to a vertical line, the swing arm length distance away from the contact point to an instantaneous center. This ensures that the tire and all linkages are rotating about the same center of zero velocity. This way no components are in bending or see any eccentric loading.

The FVSA is tuned based on a balance of roll camber and heave camber gain as the car drives. Equation 13 gives the equation for heave camber gain based on front view swing arm length:

$$\text{Heave Camber} = \tan^{-1} \frac{1}{FVSA} \quad (13)$$

Where Heave Camber is the change in camber per each inch of wheel travel [deg/in], and FVSA is the front view swing arm length [in]. From this equation, a shorter FVSA will produce a larger camber gain for each inch of bump, and a longer arm will produce less change [2, p. 615]. Figure 21 shows a graphical representation of this relationship.

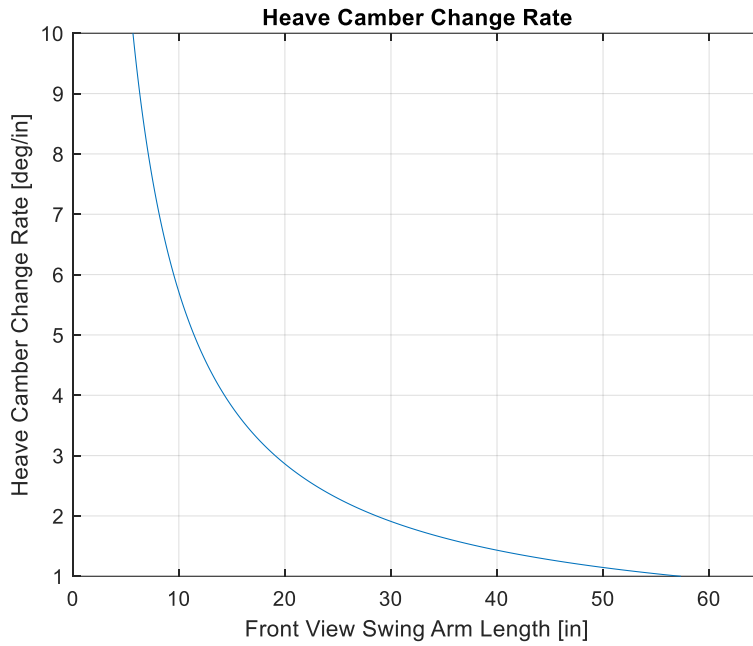


Figure 21: The Heave Camber Change Rate

The second equation deals with roll camber.

$$\text{Roll Camber} = 1 - \frac{t}{2 * FVSA} \quad (14)$$

Where Roll Camber is the wheel camber angle over the chassis roll angle [deg/deg], and FVSA is the front view swing arm length [in] [2, p. 628]. Figure 22 shows this relation graphically.

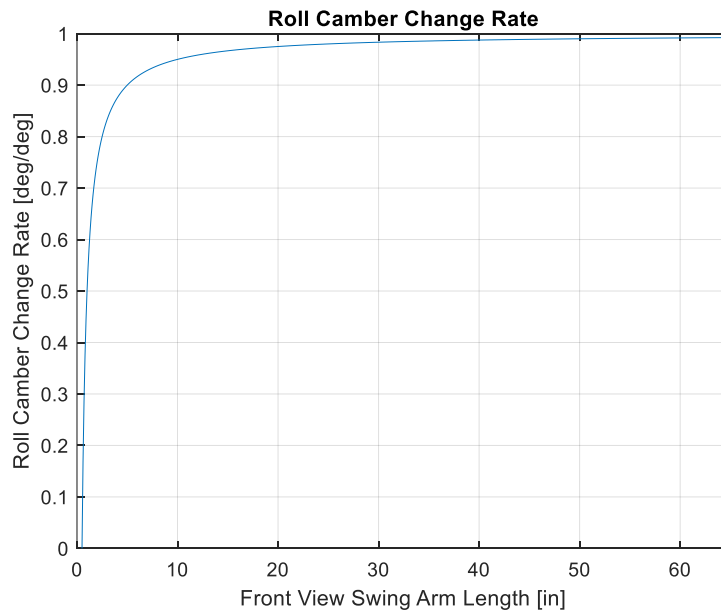


Figure 22: The Roll Camber Change Rate

Because WUFR-19 does not have an aero kit, and the competition track is generally smooth, heave camber is prioritized below roll camber. Both, however, must be considered. After calculating maximum body roll angle from stiffnesses, roll and ride rates, and other characteristics documented in MATLAB, the front and rear FVSA values were determined [15]. These data, as well, as the MATLAB generated camber change rates are in Table 9.

	FVSA [in]	Static Camber [deg]	Roll Camber Gain [deg/deg]	Heave Camber Gain [deg/in]
Front	43.07	-3	-.43	-1.33
Rear	78.93	-2	-.7	-.73

Table 15: FVSA and Camber Characteristics for the Front and Rear

The front roll camber gain was chosen to be less than the rear camber gain as the static value is larger in the front. Additionally, this will produce more consistent grip on the front tires with applied roll from lateral force through the tires. The heave camber values were considered as the roll camber was iterated but were ultimately derived not set.

Figure 23 shows the final front view geometry for the front suspension. Most notably, the instantaneous centers are above ground and inboard of the track.

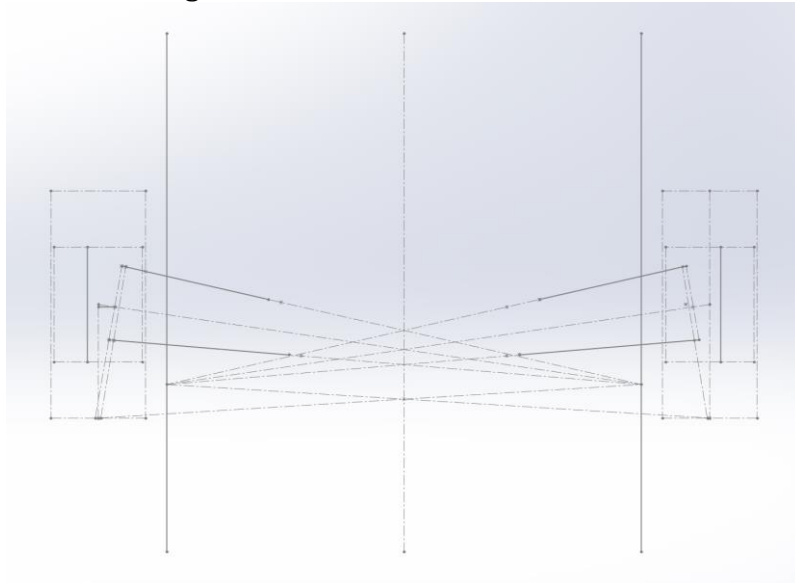


Figure 23: The Final Front-Front View Geometry

Figure 24 shows the final front view geometry for the rear suspension.

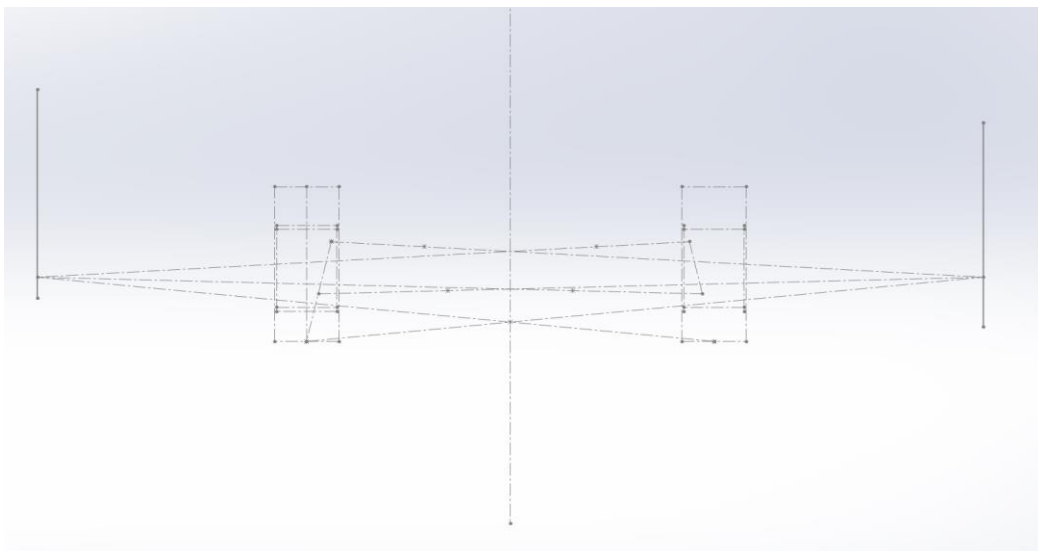


Figure 24: The Final Rear-Front View Geometry

6.2 Additional Points and Steering Geometry

Figure 25 highlights important additional geometric constraints for developing a suspension geometry. Specifically, it defines the orientation of caster angle, kingpin angle, scrub radius, and mechanical trail.

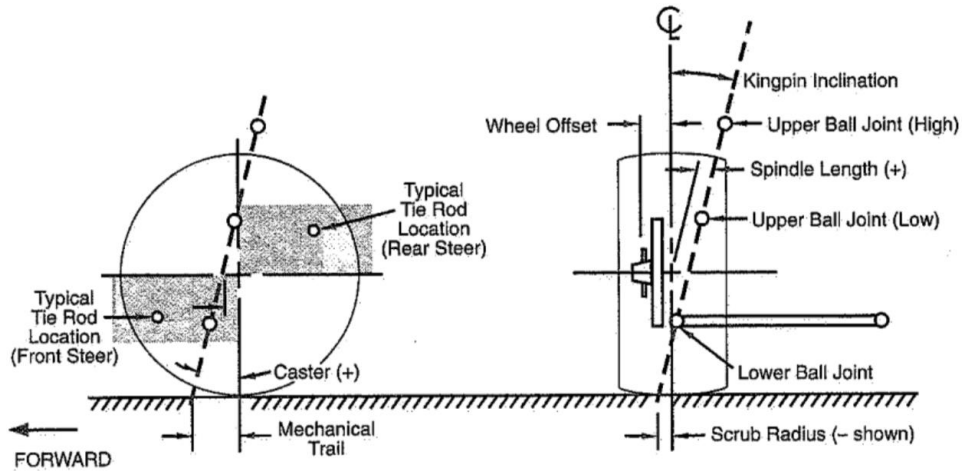


Figure 25: Important Placement of Components within the Wheel

6.2.1 Caster and Kingpin Angle

As noted in Figure 22, caster is the angled offset between the upper and lower ball joints in the side view of the wheel. Additionally, kingpin is the angled offset between the ball joints in the front view. Caster should be avoided in the rear as it creates an undesirable mechanical trail. Kingpin can be used to exploit easier packaging, so long as it does not inflate the scrub radius too high.

In the front, these two characteristics set the camber curve under the steering motion. In depth discussion of the WUFR-19 steering system can be found in Design Considerations of an FSAE Steering System [25], however, the placement of the ball joints is crucial to completing the suspension geometry.

Using data from the steering system, our maximum steering angles for optimized Ackermann were found to be, for the left front tire, -33 degrees towards the left and 25 degrees to the right. Using these values, and a relation for caster, kingpin, and camber, Equation 15 was optimized with tire data.

$$\text{Steer Camber} = K * (1 - \cos(\delta)) - (C * \sin(\delta)) - s \quad (15)$$

Where Steer Camber is the camber achieved at a given steering angle [deg], δ is the wheel steering angle [deg], K is the kingpin inclination [deg], C is the caster angle [deg], and s is the static camber [deg].

Table 10 shows all of these values for the front suspension.

	Left Turn Angle [deg]	Right Turn Angle [deg]	Kingpin [deg]	Caster [deg]	Static [deg]	[Peak, Peak] Camber
Front	-33	25	9.37	2.5	-3	[-3.18, -13]

Table 16: The Steer Camber Characteristics for the Front Suspension

Figure 23 shows the same data in graphical form. It is important to note that the main design consideration was ensuring that the inside wheel did not become positively cambered during extreme steer. This causes a drastic loss of grip and tire support under heavy lateral loading. These balance of kingpin and caster brought the camber curve close to neutral (where tire data indicates peak grip) without going over and leaving some room for manufacturing tolerances.

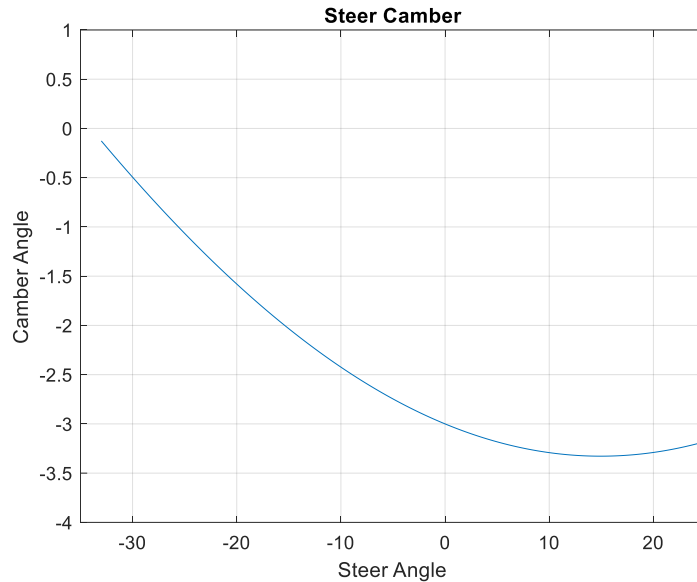


Figure 26: The Steer Camber Curve

7 OptimumKinematics Results

For final analysis, the suspension was modeled in OptimumKinematics. Before simulations, each motion had to be designed. Figure 27 shows the heave motion with the rules-compliant 50mm of total travel. The system is modeled for 1 inch (25mm) of compression travel, and 1 inch (25mm) of rebound travel. Additionally, for all motions the simulation was overridden for a cubic spline to smooth the motion path.

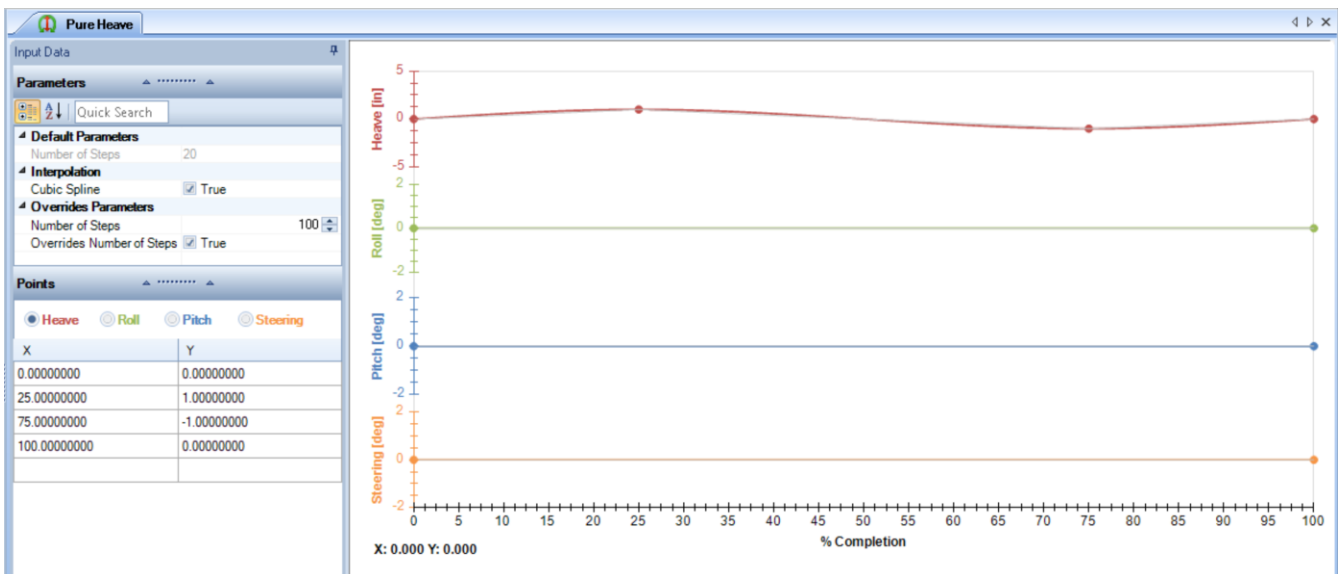


Figure 27: The Heave Motion Modeled in OptimumKinematics

Figure 28 shows the roll motion with a conservative 2 degrees of roll in either direction.

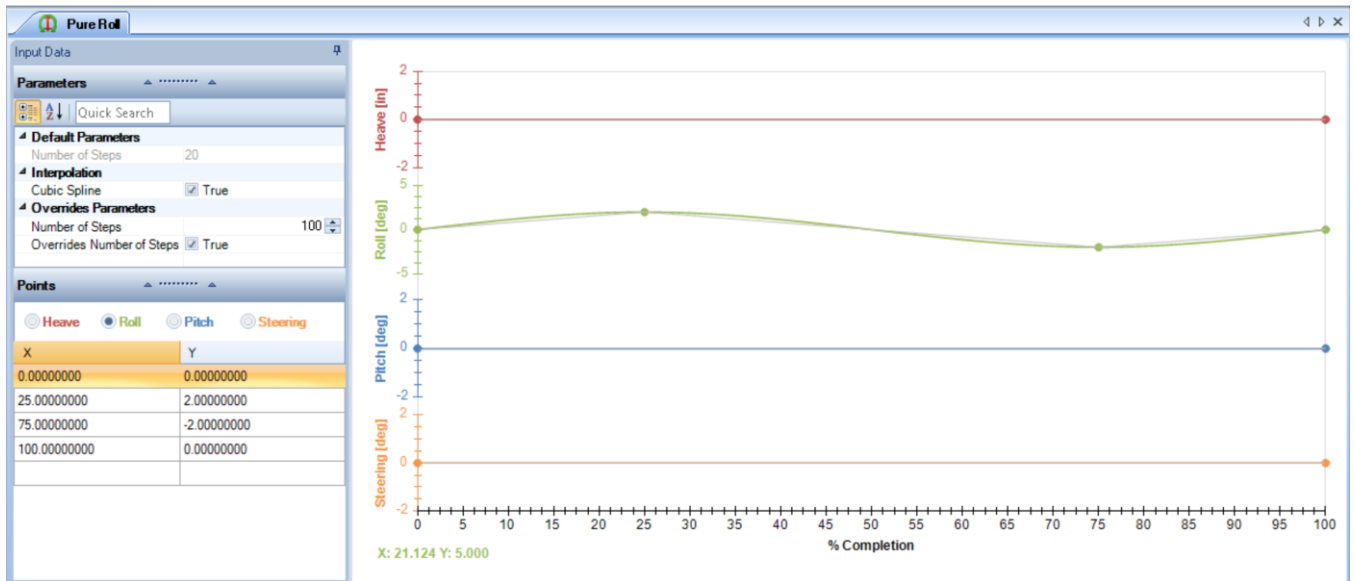


Figure 28: The Roll Motion Modeled in OptimumKinematics

Figure 17 shows the pitch motion. The front suspension is modeled in Figure 29. The front utilizes a pull rod damper actuation that is designed for a 1.5 inch ride height (for jounce clearance and front wing prototype testing) and 1 inch of static damper compression. Additionally, the black reference point in the figure is the chassis mount for the front dampers to ensure they are angled properly into the triangulated node. The pull rod is actuated from the upper control arm. The pull rod axis is aligned to go through the upper ball joint to reduce compliance and bending between the pull rod mount and the upright assembly within the wheel.

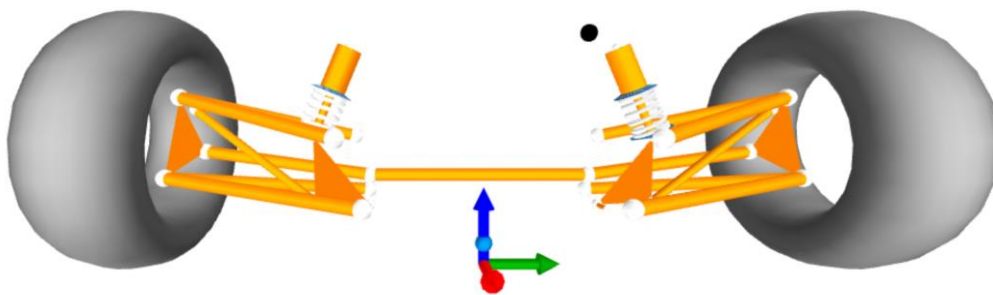


Figure 29: A Front View of WUFR-19's Front Suspension Modeled in OptimumKinematics

Figure 30 shows a top view of the front suspension.

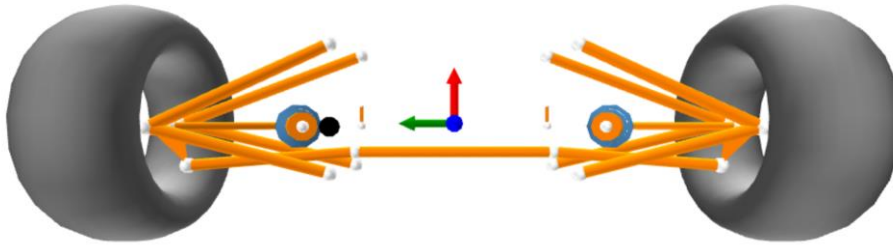


Figure 30: A Top View of WUFR-19's Front Suspension Modeled in OptimumKinematics

Figure 31 shows a front view of the rear push rod suspension with 1.5 inch ride height and 1 inch of static damper compression. The push rod is actuated from the lower control arm. Additionally, the push rod axis is aligned to the lower ball joint to reduce compliance and bending.

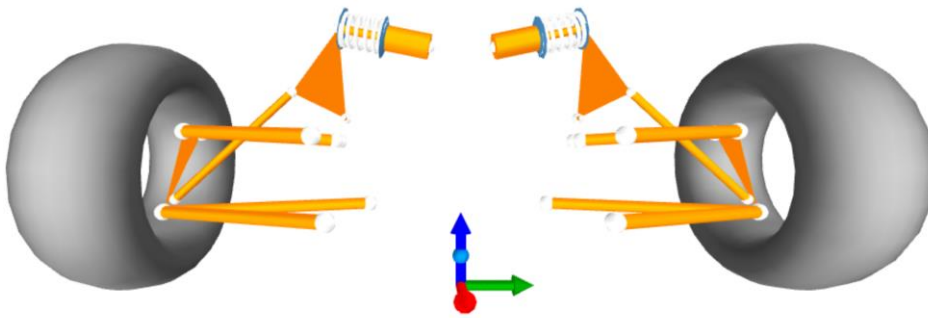


Figure 31: A Front View of WUFR19's Rear Suspension Modeled in OptimumKinematics

Figure 32 shows a top view of the rear suspension.

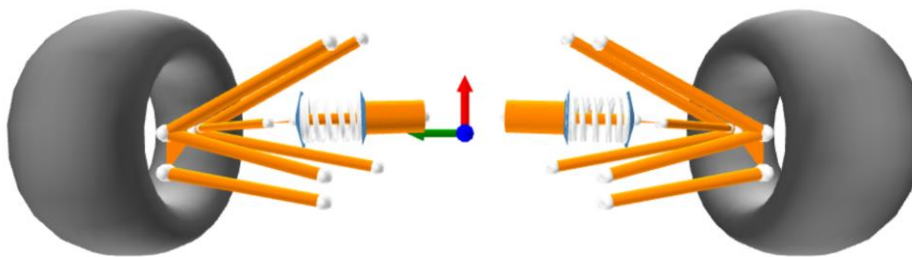


Figure 32: A Top View of WUFR-19's Rear Suspension Modeled in OptimumKinematisc

Error! Reference source not found. shows the change in camber angle of the front left wheel through the heave motion. As the heave motion becomes positive, the chassis goes up (or the wheel goes down) [18, p. 70]. This would be the wheel falling into a pot hole or rebounding from a bump. Under this motion, the tire becomes positive and will have more grip.

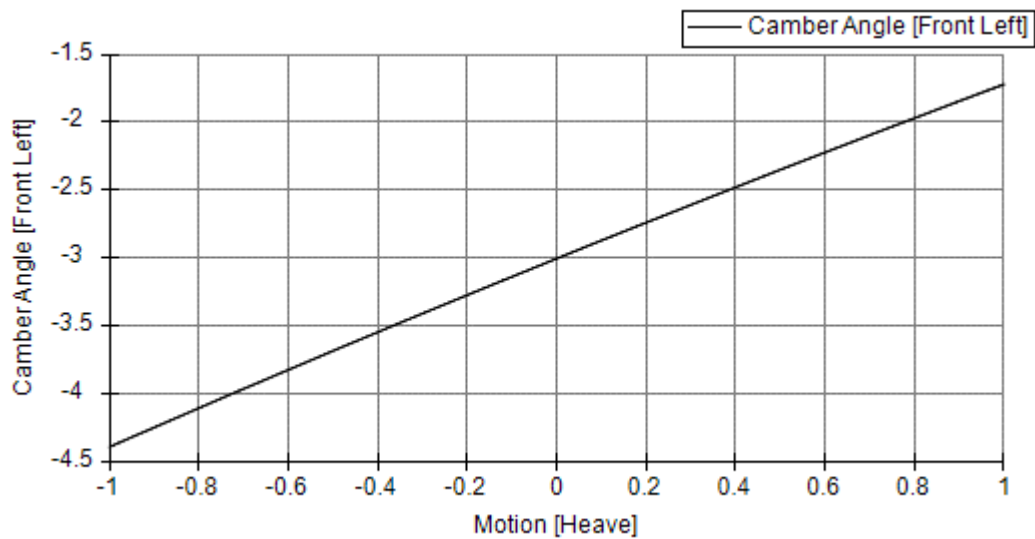


Figure 33: A Graph of Front Left Camber Gain [deg] Against the Heave Motion [in]

Figure 34 shows the camber variation for the front left wheel through the pitch motion. There was little done to tune this graph because the team does not run anti-dive or anti-squat geometry. As a result, it was ensured that the tire never approached positive camber and did not run-off towards negative camber too steeply. As the pitch motion becomes positive, the front of the car goes down (as in braking) [18, p. 70]. As a result, the car's front wheel will have some loss in grip in the lateral direction under braking. Because of this, the car should not be steered extensively under braking. Instead, the drivers should accelerate, enter a braking zone, drop the pedals, steer the wheels, and reengage the throttle.

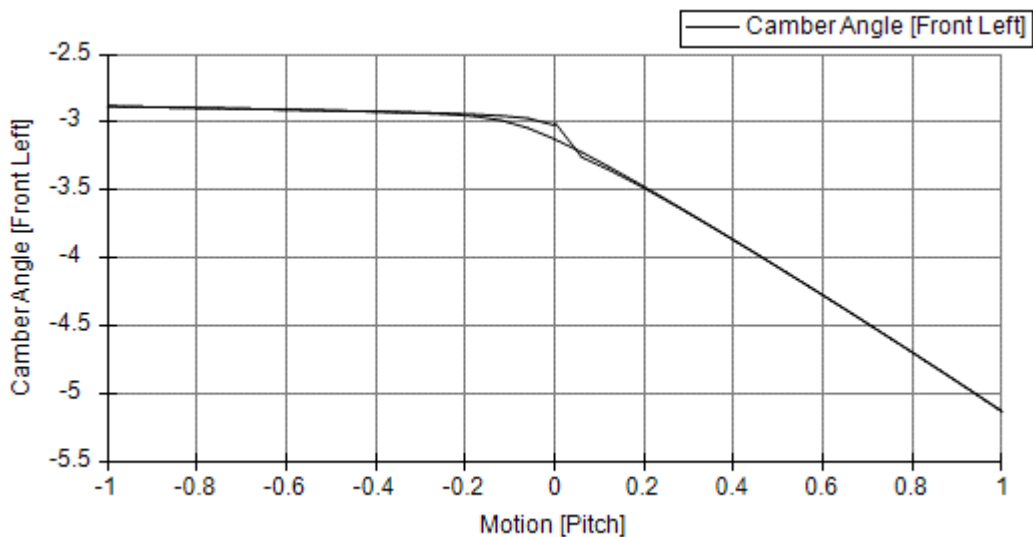


Figure 34: A Graph of Front Left Camber Gain [deg] Against the Pitch Motion [deg]

Figure 35 shows the camber curve for the roll motion of the car on the front left wheel. Positive roll is when the car rolls left in a front view [18, p. 70]. Under roll (usually induced by steer), the

tires will gain and lose a symmetric amount of camber through the entire range of motion. This should give a consistent response for right and left hand turns.

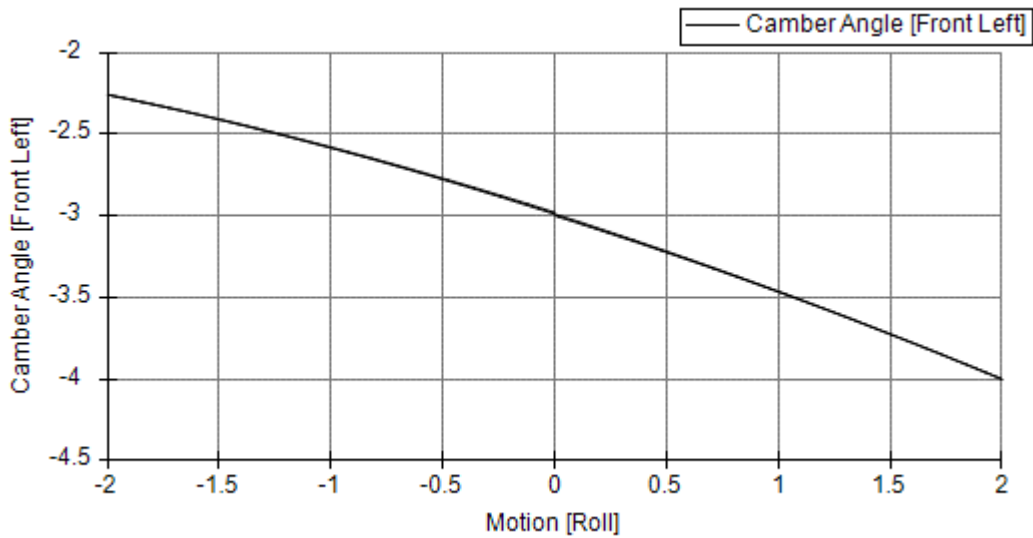


Figure 35: A Graph of Front Left Camber Gain [deg] Against the Roll Motion [deg]

Figure 36 shows the toe angle variation on the rear left tire during the heave motion. This phenomenon is known as bump steer – one of the least desirable characteristics in racing. When the rear wheel goes through vertical motion, the toe link should completely brace the fifth degree of freedom for the wheel. On the BFR-18, the toe link was not properly grounded to the chassis (it ran parallel to one linkage of the upper control arm) and the wheel had roughly 5 degrees of bump steer variation. For the WUFR-19, this was reduced to less than .2 degrees. Ideally, this characteristic would be 0, however, due to fitment within the wheel, this is impossible. The further the toe link mounts from the upper ball joint on the upright, the better braced the wheel will be. The toe link alignment can be seen in Figure 32.

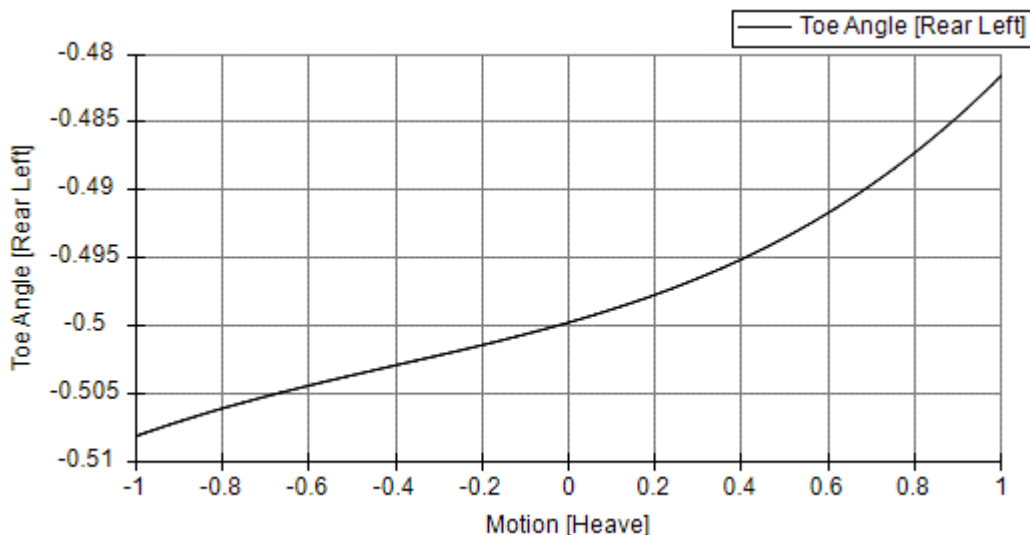


Figure 36: A Graph of Rear Left Toe Angle [deg] Against the Heave Motion [in]

Figure 37 shows the same steer variation for the rear left wheel through the pitch motion. Under acceleration, the rear tires are heavily loaded as weight is transferred rearward. As a result, toe

variation needs to be low to maintain consistent wheel heading for better off-the-line acceleration.

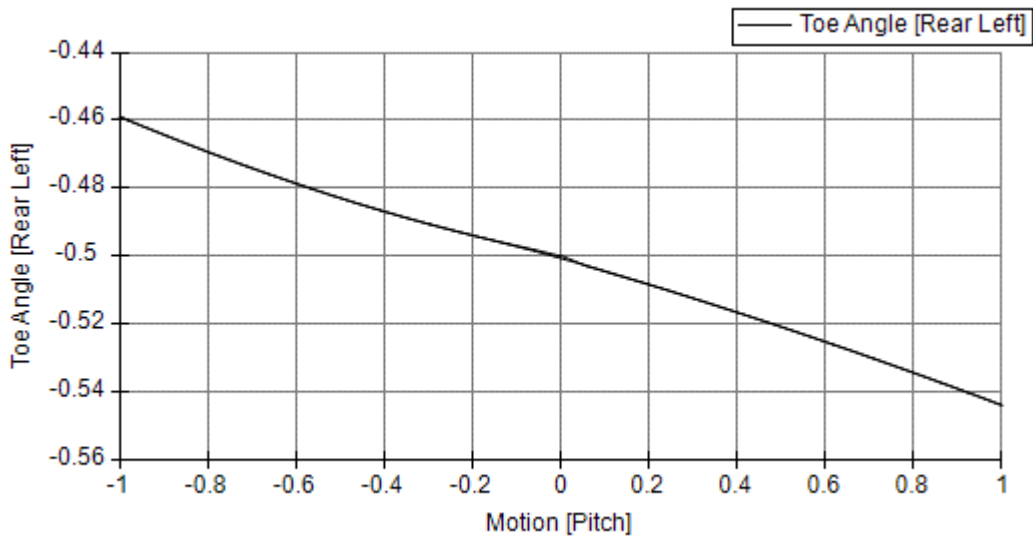


Figure 37: A Graph of Rear Left Toe Angle [deg] Against the Pitch Motion [deg]

Figure 38 shows the toe angle variation for the rear left wheel under roll. As weight is transferred laterally when the car rolls, the rear tire needs to stay true to the driver’s intended heading for optimal skidpad, autocross, and endurance performance.

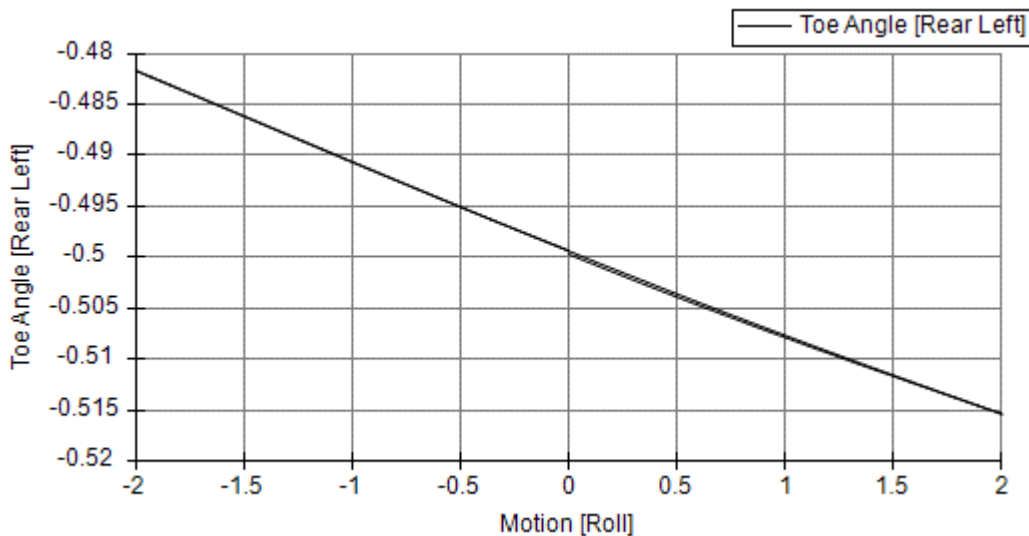


Figure 38: A Graph of Rear Left Toe Angle [deg] Against the Roll Motion [deg]

Figure 39 shows the motion ratio of the front left wheel through the heave motion. In OptimumKinematics, the motion ratio is defined as:

$$MR = \frac{\text{wheel displacement}}{\text{spring displacement}}$$

A linear 1:1 motion ratio is important for performance for several reasons. First, rules require 50 mm of travel and the team’s Ohlins TTX25 MkII dampers only have 57 mm of travel. Any significantly higher motion ratio will make the car noncompliant. Additionally, for a car with no aero package, this ensures the most efficient damping system.

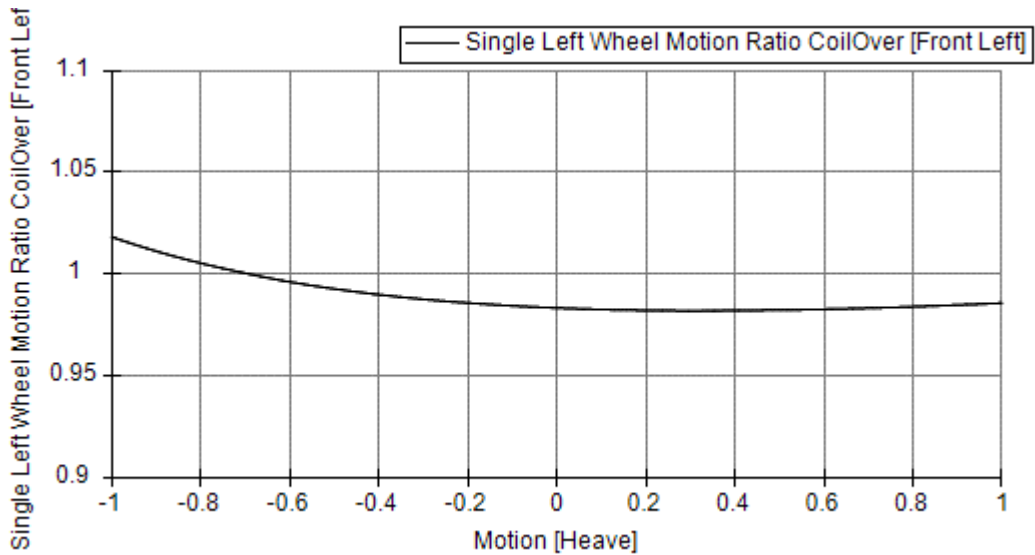


Figure 39: A Graph of Front Left Motion Ratio [unitless] Against the Heave Motion [in]

On top of motion ratio, the driver relies on feeling of wheel rate, or the spring rate experienced at and by the wheel defined as [14, p. 88]:

$$WR = MR^2 * K \tag{16}$$

Where MR is the motion ratio [unitless], WR is the wheel rate [lbs/in], and K is the installed spring rate [lbs/in]. If the motion ratio varies significantly from 1, the wheel rate will vary drastically from the installed rate. Figure 40 shows the wheel rate for a constant spring rate and varied motion ratio

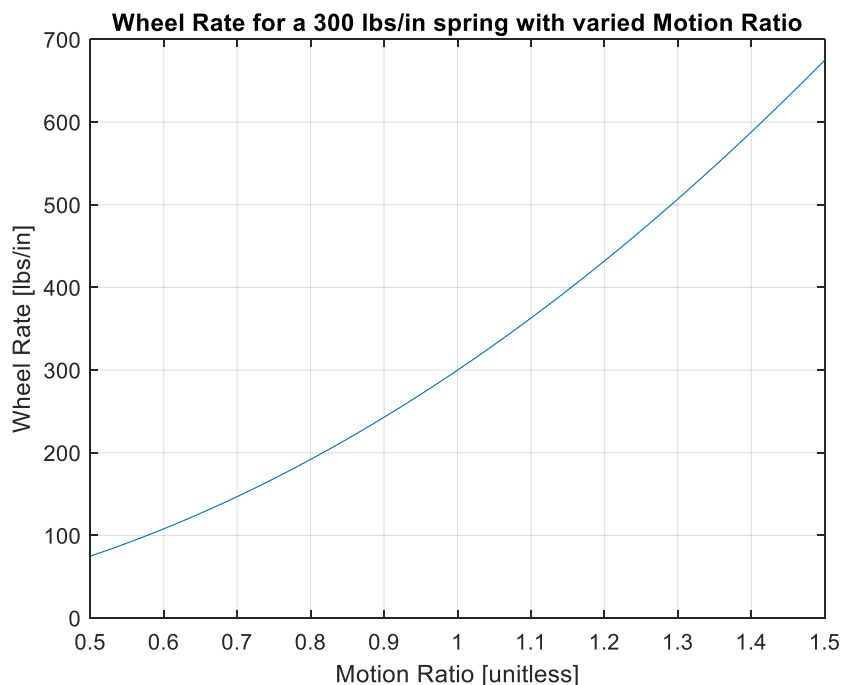


Figure 40: A Plot of Wheel Rate [lbs/in] with Varied Motion Ratio [unitless] and Constant Spring Rate

As the motion ratio diverges from 1, the real feel at the wheel becomes drastically different than the installed spring. As a result, the system becomes inefficient and the benefit of stiffer or looser springs becomes less appreciable. For a car with a significant aero package, a progressive motion

ratio (generally getting stiffer as compression increases) benefits ground clearance and increasing downforce as the car accelerates and rolls.

Figure 41 shows the motion ratio for the front left wheel under the pitch motion.

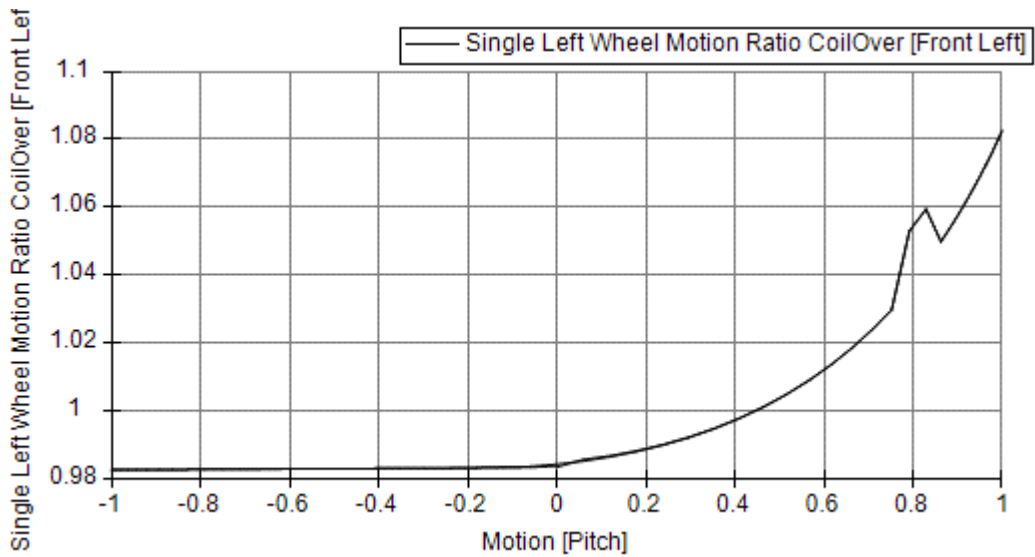


Figure 41: A Graph of the Front Left Motion Ratio [unitless] Against the Pitch Motion [deg]

Figure 42 shows the motion ratio for the front left wheel as the car goes into roll. The car has a symmetric response under roll which will provide predictable driver control through right and left turns.

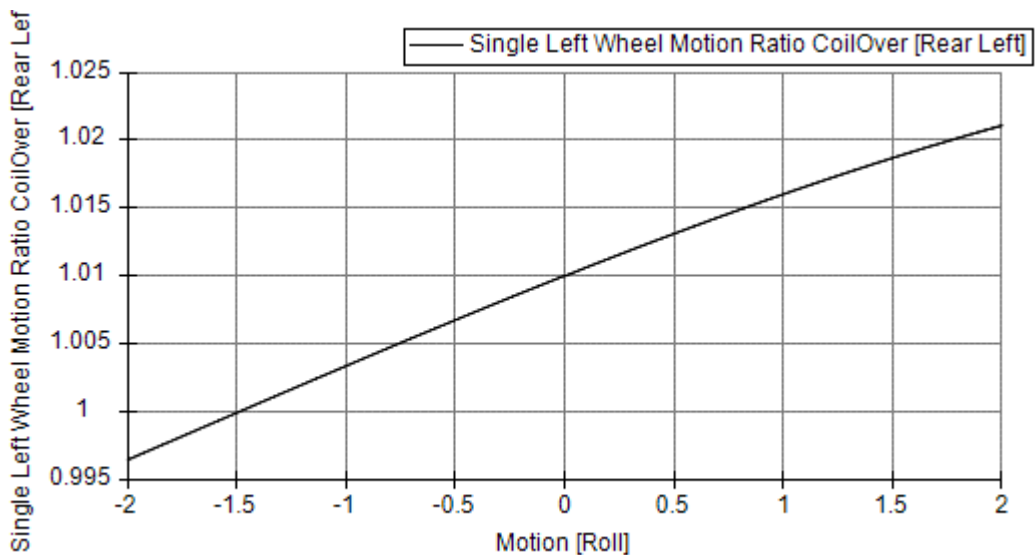


Figure 42: A Graph of the Front Left Motion Ratio [unitless] Against the Roll Motion [deg]

Figure 43 and Figure 44 show the location of the front and rear roll centers under right and left roll. As noted earlier, the front roll center is statically at 1.5 inches above the ground and the rear roll center is 2.25 inches above the ground. These figures show that the roll centers move in the same direction under the roll and that the axis stays at the same rake through the entire travel. If the axis were to invert in either the Y-Z plane or the Z-X plane, the roll geometry would have to change to ensure that the car could be handled under steering. Additionally, both graphs are generally symmetric so that roll characteristics will be consistent through right and left turns.

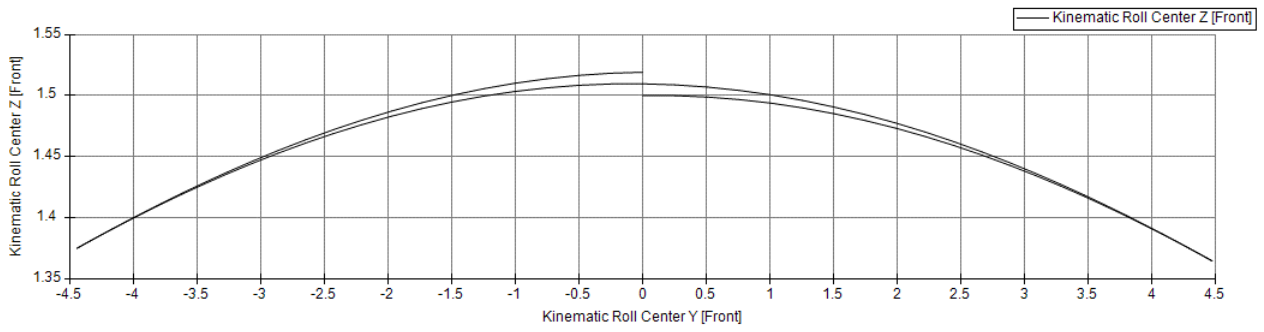


Figure 43: A Graph of the Front Kinematic Roll Center Position in Z [in] Against Y [in] Under the Roll Condition

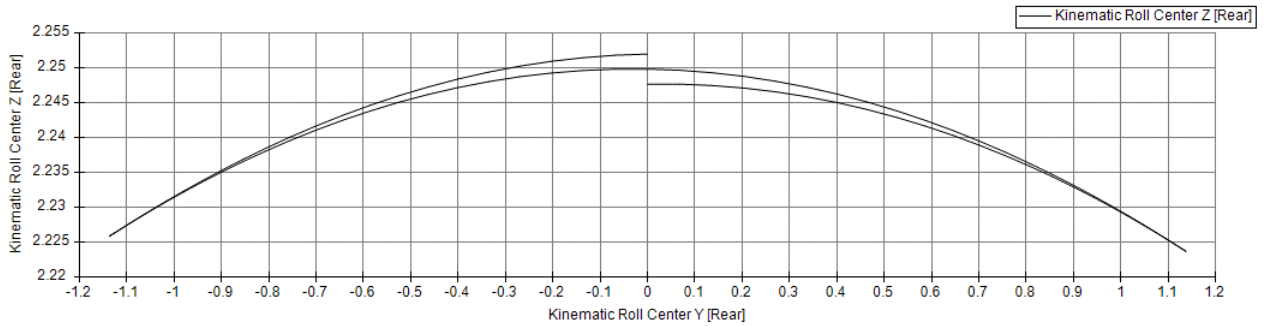


Figure 44: A Graph of the Rear Kinematic Roll Center Position in Z [in] Against Y [in] Under the Roll Condition

Going Forward

This report is not an exhaustive directory of suspension characteristics or analysis, nor is the rationale for every parameter ironclad. There are infinite combinations of correct suspension characteristics that can create a geometry for a given chassis, aerodynamic setup, and team design constraint. Going forward, this design should be reevaluated, further validated with physical tire and kinematic tests, and iterated on to continually improve performance of the car.

Appendix A: Additional Technical Information

A.1: Spring Rates

The matrix \overline{K}_s shows the available spring rates for the Ohlins TTX25 MkII dampers.

$$\overline{K}_s = \begin{bmatrix} 100 & 150 & 175 \\ 200 & 250 & 275 \\ 300 & 350 & 375 \\ 400 & 450 & 550 \end{bmatrix} \frac{lbs}{in}$$

References

- [1] C. Smith, Tune to Win: The Art and Science of Race Car Development and Tuning, Fallbrook, CA: Aero Publishers Inc, 1978.
- [2] D. L. a. W. F. Milliken, Race Car Vehicle Dynamics, Warrendale, PA: SAE, 1995.
- [3] Society of Automotive Engineers, "Formula SAE Rules 2019 V1.0," SAE, Brooklyn, MI, 2018.
- [4] Society of Automotive Engineers, "Formula SAE Design Judging Score Sheet," SAE, Brooklyn, MI.
- [5] FSAE, "Series Resources: AutoX Event Map," Society of Automotive Engineers, 2018. [Online]. Available: <https://www.fsaeonline.com/cdsweb/gen/DownloadDocument.aspx?DocumentID=49236ffb-e7fa-4fd6-a810-d50e39e005b8>.
- [6] FSAE, "Series Resources: Endurance Map," Society of Automotive Engineers, [Online]. Available: <https://www.fsaeonline.com/cdsweb/gen/DownloadDocument.aspx?DocumentID=bd2822bd-28f5-4214-8343-cda77af18b41>.
- [7] C. Smith, Prepare to Win: The Nuts and Bolts Guide to Professional Race Car Preparation, Fallbrook, CA: Aero Publishers Inc, 1975.
- [8] C. Smith, Engineer to Win: The Essential Guide to Racing Car Materials and Technology, Fallbrook, CA: Aero Publishers Inc, 1984.
- [9] J. C. Dixon, Suspension Geometry and Computation, Wiltshire, Great Britain : John Wiley and Sons , 2009.
- [10] D. C. B. a. J. D. Fieldhouse, Automotive Chassis Engineering, Leeds, UK: Springer, 2018.
- [11] R. N. Jazar, Vehicle Dynamics: Theory and Application, 2nd ed., New York, NY: Springer, 2014.
- [12] W. R. Pasterkamp, The Tyre as a Sensor to Estimate Friction, Netherlands : Delft University Press, 1997.
- [13] L. Setright, Automobile Tyres, London, UK: Chapman and Hall, 1972.

- [14] J. C. Dixon, *The Shock Absorber Handbook*, 2nd ed., Wiltshire, Great Britain: John Wiley and Sons, 2007.
- [15] A. Levy, *Determination_of_Suspension_Parameters_and_Design.m*, St. Louis, MO: WashU Racing, 2018.
- [16] A. Levy, *SU-93001-BA.SLDPRT*, St. Louis, MO: WashU Racing, 2018.
- [17] A. Levy, *WashU_Formula_Racing_2019.02Pro*, St. Louis, MO: WashU Racing, 2018.
- [18] OptimumG, "Optimum Kinematics Help File," [Online]. Available: http://www.optimumg.com/docs/OptimumKinematics_Help_File.pdf. [Accessed July 2018].
- [19] Milliken Research Associates, "Formula SAE Tire Test Consortium: Introduction," Milliken Research Associates, 1 August 2018. [Online]. Available: <http://www.millikenresearch.com/fsaettc.html>. [Accessed August 2018].
- [20] OptimumG Vehicle Dynamics Solutions, "Claude Rouelle's 101 Tips for Formula Student Competition Participants," OptimumG, Centennial, CO, 2018.
- [21] J. Speer, *Formula SAE and Hoosier Racing Tires 2018*, Plymouth, IN: Hoosier Racing Tire, 2018.
- [22] E. M. Kasprzak, *Formula SAE Tire Test Consortium (FSAE TTC) -- Round 8 Run Guide*, Buffalo, NY: Calspan Tire Research Facility (TIRF), 2018.
- [23] Wash U racing, *Hoosier 10 in R25B.OTPro*, St. Louis, MO: Wash U Racing via FSAE TTC, 2018.
- [24] A. Levy, *Lateral Force Calculator.xlsx*, St. Louis, MO: Wash U Racing, 2018.
- [25] C. McRae, "Design Considerations of an FSAE Steering System," Wash U Racing, St. Louis, MO, 2018.
- [26] Calspan Tire Research Facility (TIRF), *Formula SAE Tire Test Consortium (FSAE TTC)*, 2018.
- [27] OptimumG: Vehicle Dynamics Solutions, "OptimumKinematics Generic FSAE Case Study," OptimumG, Brooklyn, MI, 2015.